TAMPEREEN TEKNILLINEN YLIOPISTO
TAMPERE UNIVERSITY OF TECHNOLOGY

Juho Väisänen

Methods for Analysing the Sensitivities of Bioelectric Measurements

Julkaisu 888 • Publication 888

Tampere 2010

Tampereen teknillinen yliopisto. Julkaisu 888
Tampere University of Technology. Publication 888

Juho Väisänen

Methods for Analysing the Sensitivities of Bioelectric Measurements

Thesis for the degree of Doctor of Technology to be presented with due permission for public examination and criticism in Rakennustalo Building, Auditorium RG202, at Tampere University of Technology, on the 4th of June 2010, at 12 noon.

Tampereen teknillinen yliopisto - Tampere University of Technology
Tampere 2010

ISBN 978-952-15-2361-8 (printed)
ISBN 978-952-15-2382-3 (PDF)
ISSN 1459-2045

ABSTRACT

In the 21st century the trend in healthcare is towards the early detection and prevention of disease and from hospitalization to increased personalization. The novel wearable and implantable systems for electrocardiographic (ECG) and electroencephalographic (EEG) measurements are being developed to enable monitoring of people during their everyday lives or in emergency situations.

The objectives of these novel devices and bioelectrical measurements in general are to register signals arising from a certain region of interest (ROI). The aim might be to direct the measurement to a limited area of the cardiac muscle, such as an apical region of ventricles. This is of particular interest when monitoring different cardiac arrhythmias or changes in activation of a certain segment of the myocardium after infarction. The sensitivity of an ideal measurement should give greater and more intense focus on these target areas than on other areas of the volume conductor, thus yielding more specific and better quality measurements. When designing novel measurement devices and setups it would be beneficial to know where to locate the electrodes in order to measure the target signals and monitor their source regions as efficiently as possible. This is especially important in the application of wearable or implantable measurement systems when there is a limit to the number and location of recording electrodes.

The selection of the electrode system should be based on quantitative analysis of certain characteristics such as sensitivity distributions. Because different electrode setups are suitable for different measurement purposes or conditions it would be beneficial to be able to evaluate their sensitivity properties before conducting the actual measurements. The modelling of bioelectric measurements provides an effective means of studying sensitivity distributions.

The present thesis introduces a novel quantitative analysis method called region of interest sensitivity ratio (ROISR) for the evaluation of bioelectric measurement setups through the modelling of sensitivity distributions. ROISR is applied to analyse the specificity of EEG and ECG measurement setups to a certain ROI within brain and heart. Using simulations and measurements, the thesis proposes that the ROISR method developed here has a strong correlation to the signal-to-noise ratio (SNR) of a measurement and thus provides an efficient tool for the analysis and development of bioelectric measurement setups.

In the thesis the sensitivity distribution analysis is also applied to the analysis of the effects of the dimensions of an implantable ECG device on measurement. The interelectrode distance was found to be the major factor in implant design that determines sensitivity. Other parameters related to implant dimensions have only a minor effect on the average sensitivity of the measurement. It was also observed here that implanting the electrodes deeper under the skin has major effects on the local sensitivities in heart muscle which may affect the morphology of the measured ECG.

ACKNOWLEDGEMENTS

The thesis work has been carried out in the Department of Biomedical Engineering, Tampere University of Technology, (the former Ragnar Granit Institute).

I wish to express my gratitude to my supervisor, Professor Jari Hyttinen PhD, for his guidance throughout my career as a researcher. He introduced me to the fascinating world of modelling and gave me a unique opportunity to participate the development of implantable ECG devices.

I wish to thank all my co-authors for their efforts and valuable contributions to my research during these years. I am also indebted to all other colleagues who have provided such an inspiring working atmosphere.

I wish to thank Professor Rob MacLeod, PhD, (University of Utah, USA) and Professor R. Martin Arthur, PhD, (Washington University in St. Louis, USA) for their constructive criticism and advice as examiners of this thesis. I also wish to thank Jari Viik, PhD, for his valuable comments during the preparation of the thesis manuscript. I also thank Alan Thompson, MPhil, for carefully revising the English of my thesis.

The financial support of The Academy of Finland, The Finnish Cultural Foundation, The Finnish Cultural Foundation (Pirkanmaa Fund), The Emil Aaltonen Foundation, The Foundation of Technology and The Tampere City Science Foundation is gratefully acknowledged.

I would also like to thank my parents and brother for all their support and encouragement during these years. Finally, my deepest gratitude goes to my beloved wife Outi and son Eemil. They have kept my life in balance between work and leisure, and Outi as my colleague, has also valuably contributed to my research.

Pirkkala, May 2010

TABLE OF CONTENTS

LIST OF ORIGINAL PUBLICATIONS

Sensitivity properties of bioelectric measurements

[I] J. Väisänen, O. Väisänen, J. Malmivuo, J. Hyttinen: “New Method for Analysing Sensitivity Distributions of Electroencephalography Measurements” Med. Bio. Eng. Comp., vol 46. (2) pp. 101-108, 2008

[II] J. Väisänen, J. Malmivuo, J.Hyttinen: “Correlation between Signal-to-Noise Ratios and Region of Interest Sensitivity Ratios of Bipolar EEG Measurements” Med Bio. Eng Comp., vol 46. (4) pp. 381-389, 2008

[III] J. Väisänen, J.Hyttinen: “Region of Interest Sensitivity Ratio in Analyzing Sensitivity Distributions of Electrocardiographic Measurements” Ann. Biomed. Eng., vol 36. (4), pp.692-701, 2009

Implantable ECG measurements

[IV] J. Väisänen, J. Hyttinen, J. Malmivuo: “Finite Difference and Lead Field Methods in Designing of Implantable ECG Monitor” Med. Bio. Eng Comp, vol. 44, (10), pp. 857-864, 2006

[V] J. Väisänen, J. Hyttinen, and J. Malmivuo, ”Analysing Specificity of a Bipolar ECG Implant to 12 Segments of the Left Ventricle”, in proc. , Computers in Cardiology 2006, Valencia, (33), pp. 753-756, 2006

AUTHOR'S CONTRIBUTION

The author designed the studies, implemented the methods and prepared the results of all publications. The novel sensitivity distribution analysis method, ROISR, presented in publication [I] was developed in co-operation with Outi Väisänen PhD. When writing the papers the author also received valuable comments from the co-authors.

LIST OF ABBREVIATIONS

AMG	Algebraic multigrid
AMI	Anterior myocardial infarction
APD	Action potential duration
AV-node	Atria ventricular node
BSPM	Body surface potential map
CG	conjugate gradient
CSF	Cerebrospinal fluid
CT	Computed tomography
CV	Conduction velocity
DTMRI	Diffusion tensor magnetic resonance imaging
ECG	Electrocardiography
EEG	Electroencephalography
EP	Evoked potential
ERP	Evoked related potential
FDM	Finite difference method
FEM	Finite element method
FSV	Fifth sensitivity volume
GMG-CG	Geometric multigrid preconditioned CG
HSV	Half-sensitivity volume
IMI	Inferior myocardial infarction
LV	Left ventricle
MEG	Magnetoencephalography
MI	Myocardial infarction
MRI	Magnetic resonance imaging
MSD	Mean square difference
PCG	Conjugate gradient preconditioned by symmetric successive over-relaxation
PDE	Partial differential equation
PMI	Posterior myocardial infarction
ROI	Region of interest
ROISR	Region of interest sensitivity ratio
RV	Right ventricle
SNR	Signal-to-noise ratio
SOR	Successive over-relaxation
VEP	Visual evoked potential
VCG	Vectorcardiography
VHM	Visible human man
WCT	Wilson Central Terminal

∇	Gradient
$\nabla \cdot$	Divergence
α	Angle between lead vector and source vector
Φ	Scalar potential
$\boldsymbol{\sigma}$	Conductivity tensor
θ	Angular displacements from the negative z-axis
ϕ	Angular displacements from the negative xz-axis
c	Lead vector
H	Source volume
I_r	Reciprocal volume current
$\boldsymbol{J}_i$	Source current density vector
$\mathbf{J}_{LE}$	Lead current density vector
G	Sensitivity matrix
p	source vector
t	Instant of time
V_{LEAD}	Lead voltage
x	Measurement lead
y	Location within volume conductor

1 INTRODUCTION

Various electrode systems such as implantable, wearable or multilead systems are applied in measuring the electrical functions of the brain (electroencephalogram, EEG) and the heart (electrocardiogram, ECG). State-of-the-art measurement technologies enable a variety of measurements to be made both in clinical setups and in everyday life. The clinical system most widely used for monitoring the electrical activity of the heart is the 12-lead ECG system which was invented in the early 20th century (Einthoven *et al.* 1913; Wilson *et al.* 1934; Macfarlane 1989). In clinical and research setups it is possible to use a large number of measurement electrodes but with devices such as implantable or portable monitoring systems used in everyday life, it is essential to reduce their number to a minimum. Moreover, health care as well as ECG and EEG measurements are becoming increasingly personalized and individual electrode setups are needed. Different electrode setups are suitable for different measurement purposes or conditions thus it would be useful to be able to evaluate the properties of the measurements before conducting them. One could then easily select the optimal electrode system for the measurement at hand thus providing better quality measurements for diagnostic purposes. To support this selection the qualities of various electrode systems should be characterized by different parameters related, for example, to the sensitivity distributions of electrode setups.

The objective in most bioelectrical measurements is to record and analyse signals arising from sources in a certain region of interest (ROI), e.g. an ischemic region within the myocardium or an area where evoked responses are generated in the brain. The locations of the measurement electrodes have a major effect on measurement sensitivity. The sensitivity of an ideal measurement should have greater and more intense focus on these target areas than on the other areas of the volume conductor, thus yielding more specific measurements and a high signal-to-noise ratio (SNR). When designing novel measurement devices and setups it would be beneficial to know where to locate the electrodes for measuring the target signals and to monitor their source regions as efficiently as possible. There might also be a need to apply measurements concentrated at a specific area of the cardiac muscle, such as in a segment of the left ventricle (LV). Thus the electrodes should be located where the measurement is most specific to the activation arising in this source volume. This is of special interest, for example, when

monitoring different cardiac arrhythmias or changes in activation of a certain segment of the myocardium after infarctions with implantable or wearable ECG devices.

Implantation of a measurement device into the human body is an invasive, time-consuming, expensive and almost irreversible operation. This means that the effects of implantation or implant design on the measurement cannot be tested and reviewed by actually implanting the device into humans during the design process. To achieve successful measurements by implanted devices it is vital to have prior knowledge of the effects of the implantation or implant design on the measurements. There is thus a need for methods providing such information without the actual implantation of a device in test subjects, and such information would be most valuable if it was already available at the design stage.

Modelling of bioelectric measurement systems and their sensitivity distributions can provide effective tools to benefit the above mentioned cases. Modelling affords an effective means of investigating characteristics such as implant shape, dimensions and implantation location. This information would be available without expensive and time-consuming *in vivo* trials. Modelling also provides an effective means to study the sensitivity distributions of bioelectric measurements and further develop new measurement configurations yielding more accurate tools for diagnostics. Previous modelling studies of implantable cardiac devices have modelled the current distributions generated by stimulation devices such as implantable cardiac defibrillators (Panescu *et al.* 1994; Ferdjallah *et al.* 1996; Krasteva and Papazov 2002). There is thus a lack of modelling studies that focus on the measurement sensitivities of implantable ECG monitors.

Previously only a few modelling related quantitative parameters have been applied in the analysis of the sensitivity distributions of bioelectric measurements. One of these parameters has been the half-sensitivity volume (HSV) which defines the volume in which the measurement sensitivity is concentrated (Malmivuo *et al.* 1997). It has been applied in analysing the differences in EEG and magnetoencephalography (MEG) measurements (Malmivuo and Suihko 2004). Hitherto, however, no modelling methods have been introduced which can be applied to describe how well the measurement sensitivity of a measurement lead is concentrated on a certain ROI. It would be important to apply the optimal measurement configuration in order to obtain all information of these sources with high SNR. Due to a lack of such analysis methods it is difficult to compare the quality of the measurement setups with modelling-based approaches when selecting the optimal configurations for different bioelectrical measurements.

To provide analysis methods and tools for the analysis of bioelectric measurements through modelled sensitivity distributions, the present thesis introduces a novel quantitative method called region of interest sensitivity ratio (ROISR). The ROISR method is applied to describe the specificity of a bioelectric measurement to certain sources of interest, such as a segment of the myocardium. The method developed is used in the analysis of surface EEG, implantable ECG and surface ECG measurement configurations. This thesis also applies sensitivity distribution analysis to study the effects of implantation and implant dimensions on sensitivity distributions.

2 OBJECTIVES OF THE THESIS

The thesis contains two topics related to sensitivity distribution analysis methods and their applications in design and evaluation of different bioelectric measurements. The sensitivity distribution analysis provides methods for studying and assessing the properties of various bioelectric measurements.

The first topic concerns the development of a quantitative analysis method to assess the properties of measurement. The purpose is to develop a modelling analysis method to assess the specificity of a bioelectric measurement on a selected region of sources. The objectives are to:

- develop a sensitivity distribution analysis method to assess regional specificity and its relation to the SNR of a bioelectric measurement [I]
- validate the method with EEG measurement data and computer simulations [I] [II]
- evaluate the applicability of the method for analysing the ECG measurements [III]

The second topic is related to the implantable ECG measurement devices. The purpose is to provide information on implantable measurements by means of modelling and sensitivity distribution analysis. The objectives are to:

- study the effects of the implant's characteristics and implantation depth on sensitivity distributions [IV]
- study the effects of the implantation site on the specificity of the ECG implant [V]

3 REVIEW OF LITERATURE AND THEORETICAL BACKGROUND

3.1 Electrocardiography and electroencephalography

3.1.1 Heart and brain as bioelectric sources

THE HEART AS A BIOELECTRIC SOURCE

The heart consists of myocardial cells creating and/or conducting electric currents. The electrical activity of the heart is in normal conditions initiated by the sinus node which behaves as a pacemaker. The sinus node creates an action potential wavefront propagating through the atria to the ventricles causing the contraction of myocardial cells and inciting the mechanical pumping and further vital blood flow. The small electric currents raised by the myocardial cells flow intensively within the heart muscle and also throughout the whole body. These currents create millivolt level potentials between different sites in the body. The potentials can be measured with biopotential electrodes which transform ionic current flow in the body to electric current flow in wires. The ECG is basically time dependent potential differences between two electrodes located either on the body surface or inside the body. (Barr 1989)

Different diseases and abnormalities cause changes in the electrical activity of the heart and are further reflected as changes in measured ECG. Many modelling methods have been developed to investigate and understand the genesis of normal and abnormal electrical behaviour of the heart. The activation wavefront is a double layer which can be described by an equivalent dipole. The prototype model of ECG was described by Einthoven in the early 20^{th} century. In his model Einthoven described the cardiac activation by a single time varying dipole in a fixed location. Einthoven placed his electrodes in the limbs and the model was adapted to account for the potentials at these locations. The body was considered as an unbounded two dimensional volume conductor with a dipolar source at its centre. This simplistic model has served as the basis for

present clinical electrocardiography and the 12-lead ECG system. (Einthoven *et al.* 1913; Geselowitz 1989)

Einthoven handled the three dimensional heart in two dimensions but in the mid 20th century the electrical activity of the heart was already being considered as a single three dimensional electric dipole with Burger and Van Milaan (Burger and Van Milaan 1946) having studied the relation between heart-vector and limb leads with a thorax-shaped phantom. Einthoven presented the relation between cardiac dipole and lead voltages by an equilateral triangle but Burger and Van Milaan (Burger and Van Milaan 1947) showed with their thorax-shaped phantom containing lungs and spine that the relation is affected by different inhomogeneities of the body and thus the triangle is not equilateral.

The major disadvantage of a single dipole model is that it presents the activation of different myocardial sections with the same dipole. Already in the 1960s when computational resources were increasing, new models were derived to describe electrical activation of different myocardial segments with an individual dipole. Selvester *et al.* (1965) found their 20 dipole model feasible for simulation of various pathologies such as myocardial infarction (MI) or hypertrophies. In another study the distributed dipoles was shown to describe mid parts (20 to 70 ms) of QRS-activation in more detailed fashion than a single equivalent dipole (Selvester *et al.* 1968). Selvester *et al* (1965) applied dipoles which point towards the normal of the epicardial surface because the activation wavefront described earlier is moving from the endocardium towards the epicardium (Malmivuo and Plonsey 1995).

The dipolar models described above contain static dipoles in fixed locations although their dipolar moments are time dependent. These models ignore the fact that the electrical activation of the heart has a time-related trajectory. Therefore moving dipoles have been used to present the timed trajectory of cardiac electrical activation (Arthur *et al.* 1971; Gulrajani *et al.* 1984).

The moving dipole models apply one or two dipoles representing the activation of larger myocardial volumes. In order to accompany the time dependency and multiple source locations, a uniform double layer source description has been applied. In the uniform double layer model the sources are assumed to be of a dipolar nature at each surface element of the activation wavefront. Thus the double layer model presents an independent activation boundary containing multiple dipoles for each time instant. These sources are directed towards the tissue which is still at rest. (van Oosterom 1989)

Multipoles have also been applied to describe the electrical activity of the heart (Arthur *et al.* 1972; Malmivuo and Plonsey 1995). For instance, Arthur *et al.* (1972) modelled ECG with dipoles combined with quadrupole components and achieved better fit between simulations and measured surface potentials than when applying only dipoles in simulation.

Although the dipolar presentation of the electrical activity is simple and computationally inexpensive, it does not take into account additional information from the cellular level characteristics such as transmembrane potentials, action potential duration or

conduction velocity. These features are taken into account when representing the cardiac activation with cellular automata models (Werner *et al.* 2000; Sachse 2004; Atienza *et al.* 2005).

THE BRAIN AS A BIOELECTRIC SOURCE

The brain consists of neuronal cells creating and conducting electric currents. The postsynaptic potentials in the dendrites of large pyramidal neurons initiate electric currents. These currents initiate potentials at different sites of the head measured by EEG. Depending on the measurement site, the recorded EEG is originating from a single neuron or from large populations of neurons. The potential of a single neuron can be recorded only with microelectrodes inserted into the brain and the potential raised by population of neurons can be measured from the scalp surface. (Nunez 1981)

The electrical activity of the brain differs from the heart's activity in that in normal conditions there exists mainly two different activity types: spontaneous and evoked potentials (EP). The spontaneous activity is present at different parts of the brain tissue while EPs are responses to certain visual, motor or sensory stimulus and are generated at certain locations of the brain. For example, visual evoked potentials (VEP) are generated at the occipital brain structures as an electrical response to visual stimulus. (Nunez 1981)

Various static and moving dipole models have been applied to describe the electrical sources of the brain (Gulrajani *et al.* 1984; de Munck *et al.* 1988b; He *et al.* 2002). A single equivalent dipole has been verified to represent adequately the electrical activity of large groups of pyramidal cells (de Munck *et al.* 1988b). The spatially random dipoles as well as homogeneously distributed dipoles have been applied to describe the spontaneous background activity which is considered as noise in EP measurements (de Munck *et al.* 1992; Lutkenhöner 1998a; 1998b).

3.1.2 ECG and EEG measurement systems

ECG and EEG measurements are frequently-used diagnostic tests in everyday health care. The recordings of cardiac state with body surface ECG and brain activity with EEG are non-invasive, inexpensive and simple procedures. These measurement systems contain a different number of measurement leads. A measurement lead provides a time-dependent voltage difference between two locations on the body, i.e. ECG or EEG signals. The information on electrical activity provided by the lead is essentially dependent on the positioning of the lead. Different lead locations provide different ECG or EEG signals although the original source of activation may be the same. Thus the proper selection of measurement systems has an essential role in diagnostics.

The measurement leads can be either bipolar or so-called unipolar leads. For example, a clinical 12-lead ECG system contains 3 bipolar leads, 3 augmented unipolar leads and 6 unipolar leads. The term unipolar is somewhat misleading since the measurements are always potential differences between reference and measurement point. The difference between bipolar and unipolar is in the reference point. The bipolar lead measures the potential difference between two physical locations on the body surface, of which one is

a measurement point and the other a reference point. The unipolar leads measure the potential difference between measurement points on the body surface and, for example, a remote reference. According to Frank Wilson the remote reference should resemble the potential at infinity. In a 12-lead system the remote reference is the average potential of three limb potentials, also known as Wilson central terminal (WCT). (Wilson *et al.* 1934; Macfarlane 1989)

Clinical measurement systems are designed to measure certain specific characteristics of bioelectric activation. Different assumptions and even simplifications of electrical activity have been considered when measurement systems are constructed. For example, the clinical 12-lead ECG and vectorcardiography (VCG) systems were developed based on the assumption that electrical activity of the heart can described by an equivalent dipole in the middle of the homogeneous volume conductor. The 12-lead ECG system even contains three Einthoven limb leads which were designed to measure a two dimensional dipole located in the centre of homogenous sphere and Frank's VCG system measures three orthonormal components of this fixed heart vector. (Einthoven *et al.* 1913; Frank 1956; Macfarlane 1989)

Measurement systems can contain from one measurement lead, e.g. implantable loop recorder, to as many as hundreds of e.g. high resolution EEG (Hoekema *et al.* 1999; Oostenveld and Praamstra 2001; van Dam and van Oosterom 2007). The measurement system and the number of electrodes that should be applied ultimately depends on the clinical problem at hand (Tragardh *et al.* 2006). The information provided by these systems is determined by the number of leads and their locations on the body surface. Multilead systems containing tens of electrodes provide more spatial information on the underlying bioelectric sources and better coverage of potential distributions on the body surface than a single lead, the traditional 12-lead ECG system or 10-20 EEG system. Limited systems containing only single or a few leads are feasible in emergency or other ambulatory situations where the standard lead systems or multilead systems cannot be applied (Dower *et al.* 1988; Song *et al.* 2004; Russell and Gehman 2007; Casson *et al.* 2008).

MULTILEAD SYSTEMS

Body surface potential maps (BSPM) and high resolution EEG are multielectrode lead systems applied to measure the electrical activity of the heart and the activity of the brain. Figure 3.1 presents a BSPM ECG and high resolution EEG recordings with 256 electrodes. The basic purpose of the systems is to provide all the available information on the spread of activation over the thorax or head. The spatial accuracy of the activation on the thorax or head surface increases as the number of measurement leads increases. The reviews of BSPM applications and utility by Nadeau *et al.* (1995) and Kornreich (1997) highlight the various advantages of BSPM such as higher spatial accuracy and amount of information over a clinical 12-lead system. The advantages of the high resolution EEG systems lie on their better spatial resolution and accurate source localization capabilities (Lantz *et al.* 2003; Michel *et al.* 2004).

The major disadvantage limiting the clinical use of BSPMs is the high number of electrodes and installation time needed for measurement preparation (Kornreich 1997). The minimum number and locations of electrodes needed to construct a total-body BSPM have been investigated by several groups. These studies reported that 20-35 properly located electrodes can be applied to successfully construct total-body BSPM (Barr *et al.* 1971; Lux *et al.* 1978; Lux *et al.* 1979; Finlay *et al.* 2005; Finlay *et al.* 2006).

The BSPM methods can be applied in two different ways. Firstly, different myocardial abnormalities have typical time-related activation patterns on the body surface. Comparing abnormal and normal patterns has been found effective in diagnosing myocardial disorders, e.g. BSPM methods are more sensitive and specific in the detection of MIs than the traditional 12-lead ECG (Menown *et al.* 1998; McClelland *et al.* 2003).

Secondly BSPMs can be applied in noninvasive imaging of the electrical activity of the heart (Brooks and MacLeod 1997). The epicardial potentials are constructed by means of inverse solutions with torso models and measured BSPMs in order to efficiently and noninvasively analyze and study epicardial activity related to different abnormalities (Oster *et al*. 1997; Ramanathan *et al*. 2004; Wilber 2007; Ghanem 2007; Ghosh *et al*. 2008a; 2008b).

Noninvasive imaging can be applied to present epicardial potentials in clinical cases such as atrial flutter or right bundle branch block. Thus noninvasive imaging can be an applicable tool, for example, in the specific diagnosis of arrhythmia to determine the most suitable intervention mechanism or determination of cardiac location of localized interventions such as pacing or ablation (Ramanathan *et al.* 2004). The number of electrodes applied to the BSPM measurement also defines the feasibility of the noninvasive imaging in clinical use: Ramanathan *et. al.*(2004) , for example, applied 224 electrodes when measuring BSPMs. The 29-electrode setup, similar to the Lux-32 arrangement (Lux *et al.* 1978) has been reported to give all the relevant information for the efficient construction of epicardial potentials (Dössel *et al.* 1998).

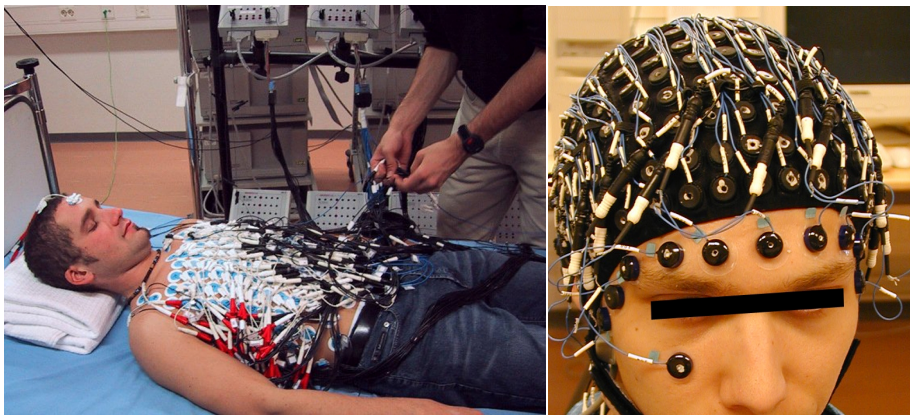

Figure 3.1 Body surface potential mapping (left) and high resolution EEG (right) with 256 leads.

AIMED LEAD SYSTEMS

Diseases such as MI and ischemia can change activation locally, for example, only on the inferior or anterior myocardium. Clinical 12-lead ECG and VCG systems were designed to present features of a single equivalent heart dipole in a fixed location and therefore they are not especially sensitive to a single myocardial region (Einthoven *et al.* 1913; Frank 1956). Aimed lead systems are needed to efficiently measure certain parts of the active myocardium. These systems have multiple applications including efficient diagnostic and discrimination between diseases, such as ischemia and infarction (Kornreich *et al.* 1985; Horacek *et al.* 2001). The objective of all aimed leads is to provide a system which is sensitive to a selected source region while also being insensitive to all other sources within the volume conductor.

Dipole models have been assigned to describe activation of different myocardial sections by separate dipoles and further study the ECG lead sensitivity to a limited region of the myocardium. Fischmann and Barber (1963) applied a torso tank model to design a resistor network which produced individually dipole moments of five ventricular areas by weighting voltages measured from eight locations on the body surface. Fischmann *et al*. (1966) demonstrated with three dipoles in a torso-tank model that there exist unweighted surface leads which are sensitive and aimed at one of these three dipoles.

Geselowitz and Arthur (1971) derived aimed ECG leads by representing myocardial sources as multipole expansion in a spherical heart model. The ECG can be considered as the weighted vectorial sum of the cardiac current sources and it was demonstrated that aimed leads can be constructed by a proper weighting function.

Hyttinen (1994) applied a reciprocal lead field approach in analyzing the sensitivities of ECG leads on different areas of the myocardium and developed aimed ECG leads. Hyttinen formed aimed ECG leads by means of optimization and singular value decomposition and concluded in his thesis that “leads constructed with optimization methods had a higher local aimed relative sensitivity while the leads generated by SVD had lower contamination of all other sources”.

On the basis of a statistical analysis of BSPMs, the leads located on the upper thorax show the best capabilities for differentiating anterior infarction patients from normal subjects and the leads located at the lower left back are best suited for distinguishing inferior infarct patients from normal subjects (Kornreich *et al.* 1986). Posterior leads have been reported to improve the detection of inferior and posterior wall infarction and ischemia (Matetzky *et al.* 1998; Khaw *et al.* 1999; Somers *et al.* 2003). Different bipolar leads have also been reported to be sensitive to different ischemic and infracted regions (Quyyumi *et al.* 1986; Kornreich 1998; Horacek *et al.* 2001). Bipolar aimed EEG leads are applied in cases such as evoked responses or brain computer interfaces where the measurement is targeted at certain region of the brain (Celesia *et al.* 1993; Lou *et al.* 2008).

Although many studies have shown the benefits and capabilities of aimed leads in diagnostics they have not been fully transferred to clinical practice because of the established status of 12-lead and other clinical systems. In order to be clinically applied,

the aimed leads should be: I) superior in diagnostics compared to traditional leads systems, II) easily applicable in all diagnostic situations, III) common diagnostic criteria should be established for aimed leads.

Most of the reported aimed leads are unipolar leads, having WCT as a reference or distant bipolar leads. Aimed leads would also be valuable in wearable or implantable solutions where the WCT reference is not available.

WEARABLE AND IMPLANTABLE SYSTEMS

Trends in healthcare in 21st century show a move away from hospitalization towards personalization. Traditionally healthcare has focussed on the treatment of diseases and symptoms but recently it has been moving towards the early detection and prevention of diseases (De Rossi and Lymberis 2005; Lymberis and Dittmar 2007). In order to detect symptoms and abnormalities at an early stage people have to be monitored during their everyday life with various sensors and devices. Thus the research and development of wearable and/or implantable ECG recorders has been increasing during the first decade of the 21st century (Medtronic; TransomaMedical; Burke *et al.* 2003; Vehkaoja and Lekkala 2004; Kauppinen *et al.* 2006; Gyselinckx *et al.* 2007; Riistama *et al.* 2007; Russell and Gehman 2007; Fischell *et al.* 2008). Figure 3.2 presents an example of such research that shows an implantable ECG monitor and wearable EEG systems developed at Tampere University of Technology, Finland. The Implant has been developed for long term measurements and thus does not make use of batteries (Riistama *et al.* 2005). The wearable EEG system is intended for emergency applications (Kauppinen *et al.* 2006).

The novel wearable and implantable ECG system allows patients to be monitored effectively in their daily lives in everyday surroundings or in emergency situations. The implantable cardiac event monitors have also proved effective in detecting various cardiac arrhythmias and ECG patterns (Benditt *et al.* 2003; Chrysostomakis *et al.* 2003;

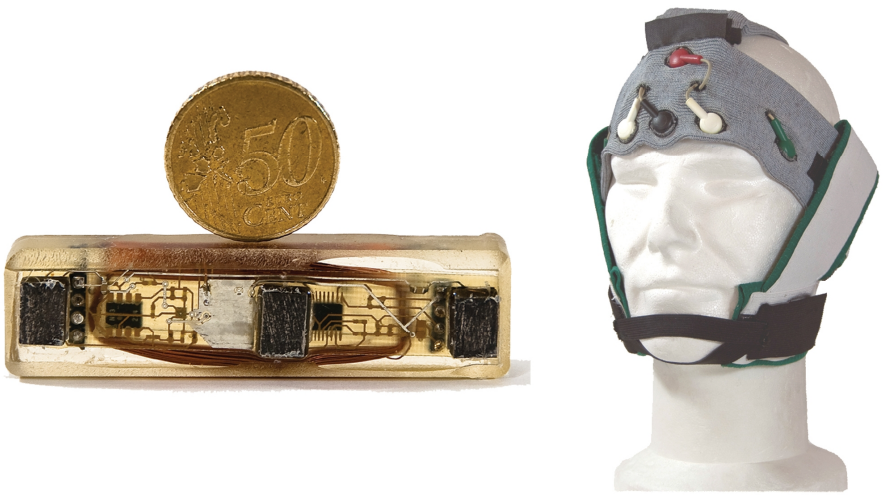

Figure 3.2 Implantable ECG monitor developed in TUT (left) (Riistama *et al.* 2007) and a wearable EEG system developed in TUT (right) (Kauppinen *et al.* 2006).

Boersma *et al.* 2004; Farwell *et al.* 2004; Song *et al.* 2004; Sarkar *et al.* 2008).

The wearable and implantable EEG systems are especially useful in emergency and critical care situations as well as in operating room conditions. Subdermal EEG systems, e.g. needle electrodes, provide high quality signals with quick installation while the wearable EEG systems are capable of recording long term EEG to facilitate various studies into areas such as monitoring epilepsy and sleep studies which can be conducted more successfully in the patient's normal environment (Ives 2005; Schneider 2006; Casson *et al.* 2008).

The limited number of leads and possible lead locations is characteristic of wearable and implantable applications. The optimal ECG lead system for smart clothing and wearable health systems contains 10 recording sites as a grid on a precordial area while also being sufficient for providing maximal ECG information (Finlay *et al.* 2008). For usability and wearability short-distance bipolar leads are often implemented in implanted and wearable solutions (Riistama *et al.* 2007; Russell and Gehman 2007). Bipolar leads with approximately 6 cm electrode separation located diagonally around standard precordial leads have been reported as suitable for QRS- and P-wave detection (Puurtinen *et al.* 2009a).

Zellerhoff *et al.* (2000) investigated the optimal locations for an implantable loop recorder, Reveal® (Medtronic Inc.). The device was subcutaneously inserted in 65 patients. The optimal implantation sites were reported to be at right or left of the sternum with vertical orientation. These locations provided the highest QRS amplitude, best visible P-wave, best measurable QRS duration and QT interval. Van Dam and van Oosterom (2007) studied subcutaneous ECG recording by simulating cardiac activation. The simulations were conducted in a male torso model containing myocardium, blood cavities, lungs and subcutaneous fat. The ECG of whole cardiac cycle was simulated by applying an equivalent double layer source model. Van Dam reported that the optimal location for implantation depends on what features of ECG are under investigation. Both of these studies also reported no significant differences between surface and subcutaneous ECG. Thus bipolar surface measurements can be applied for each patient when optimal implantation location is sought.

3.2 Modelling of Bioelectric Fields

3.2.1 Forward problem

The human body is a conducting medium where electric fields arise from bioelectric sources such as the heart and brain. Tissues of the body have their own unique dielectric properties such as conductivity and permittivity affecting the fields arising from bioelectric sources. The potential distributions within and on the human body are based on Maxwell's representations of electric and magnetic fields. Maxwell's equations can be simplified on the basis of a few assumptions. Human tissues have both capacitive and resistive characteristics affecting the current distribution on the thorax. However, it has been recognized that the ratios between conductivities and permittivities of human

tissues at low frequencies (e.g. the range of ECG) are such that the dielectric behaviour of tissues is mainly resistive (Gabriel *et al.* 1996b). Thus the quasistatic approach is accepted when the tissue properties are modelled on low frequencies (Plonsey and Heppner 1967). Equation (1) defines Poisson's and Laplace's equations that are generally used to describe bioelectric quasistatic source-field problems. Poisson's equation defines the relationships between different conductivities representing tissues and organs and the resulting potentials from different impressed sources such as cardiac or neural electric sources. A potential field $\Phi(\boldsymbol{y})$ in a bioelectrical volume conductor satisfies

$$-\nabla \cdot (\boldsymbol{\sigma}(\boldsymbol{y})\nabla\Phi(\boldsymbol{y})) = \begin{cases} \nabla \cdot \boldsymbol{J}_i(\boldsymbol{y}) = \mathrm{I_v}, & for\ \boldsymbol{y}\ in\ H \\ 0, for\ \boldsymbol{y}\ outside\ H \end{cases}, \qquad (1)$$

where y is the location within a volume conductor, $\boldsymbol{\sigma}$(y) is the conductivity tensor representing the electrical characteristics of different tissue types, containing the conductivity matrix, Φ(y) is the scalar potential at y, $\boldsymbol{J}_i(\boldsymbol{y})$ is the impressed current density at y, $\mathrm{I_V}$ is the volume source of current and H is the defined source volume, e.g. the myocardium or the brain (Plonsey 1963). Generally when bioelectric problems are solved, insulating boundary conditions are applied at the body surface. In this problem a Neumann boundary condition is applied within the surface of the model interfacing with the air. (Pullan *et al.* 2005)

The bioelectric field problems represented by Poisson's formulation can be studied by means of forward or inverse solutions. The research in this thesis has been conducted by applying a forward solution. Figure 3.3 presents examples of ECG and EEG forward problems. In the forward problem the source field, $\boldsymbol{J}_i(\boldsymbol{y})$ and volume conductor, $\boldsymbol{\sigma}(\boldsymbol{y})$, are known and the resulting potential field $\Phi(\boldsymbol{y})$ is yet to be solved. The volume conductors in ECG and EEG problems are simplified or are realistic representations of the human thorax and head. Source models can be single dipole, multidipoles, double layer, moving dipoles or cellular automata based. The solution of Poisson's equation is obtained by means of analytical or numerical calculations, depending on the complexity of the problem.

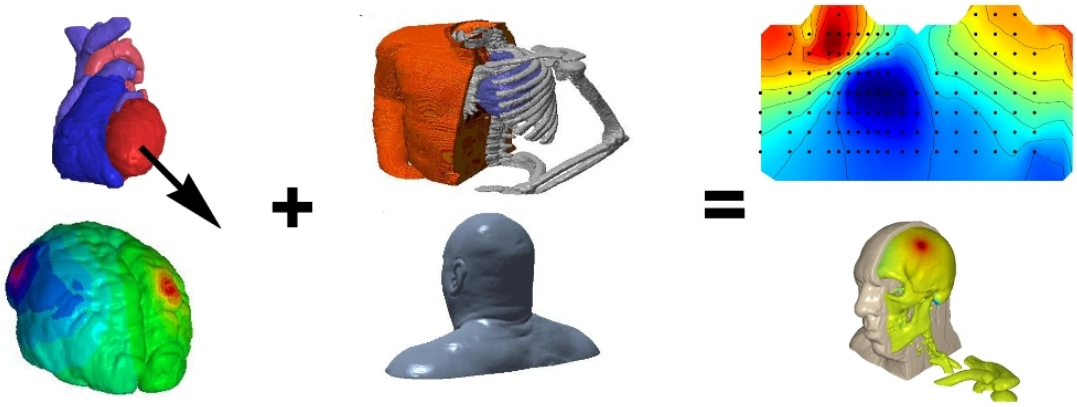

Figure 3.3 Examples of bioelectric forward problems. BSPM generated by single cardiac dipole and skull potential distribution generated by cortical sources.

3.2.2 Volume conductor models

The solution to the bioelectric problem is dependent on the following factors: 1) application, 2) computational resources available, 3) source definition and 4) anatomical volume conductor model. Level of details of anatomical volume conductor model defines the required computational resources. The spherical models are simplifications of human anatomy and enable the analytic formulation of bioelectric field calculations that require fewer computational resources than realistically shaped models (Rush and Driscoll 1969; Rudy and Plonsey 1979; Cuffin 1991; Zhou and van Oosterom 1992). The realistic models provide greater detail of anatomy and geometry but their construction also requires more work and expensive imaging resources such as magnetic resonance imaging (MRI) (Johnson *et al.* 1992; Laarne 2000). More computational resources are also needed when solving forward or inverse problems with highly realistic models containing millions of elements.

The detailed, realistic anatomical models are needed in patient-specific applications. Due to the imaging facilities and lack of computation resources, the early realistic models had low resolution and a limited number of elements. The early computer models contained only few thousand elements and only few tissue types were modelled (Selvester *et al.* 1968; Arthur *et al.* 1972; Gulrajani and Mailloux 1983; Walker and Kilpatrick 1987). In the early 1990s the Visible Human project was set to serve as a common reference of human anatomy (Ackerman 1991). The project has produced visible human male and female data sets (VHM, VHW) containing detailed anatomical structures based on computer tomography (CT), MRI and cryosection images. The available high resolution data and development of computational resources and imaging facilities have enabled modelling with detailed representations of the human body. Since the late 1980s and early 1990s multiple 3-D anatomical thorax and head models have been constructed and applied in bioelectric studies (Walker and Kilpatrick 1987; van Oosterom and Huiskamp 1989; Johnson *et al.* 1992; Lemieux *et al.* 1996; Haueisen *et al.* 1997; Kauppinen *et al.* 1998; Bradley *et al.* 2000; Laarne 2000; Sachse *et al.* 2000; Buist and Pullan 2003; van Dam and van Oosterom 2005; Fuchs *et al.* 2007; Barnes *et al.* 2008; Nöjd *et al.* 2008; Puurtinen *et al.* 2009b). Today's high resolution models contain millions of elements with tens of tissues represented (Kauppinen *et al.* 1998; Sachse *et al.* 2000; Nöjd *et al.* 2008; Yang and Patterson 2008).

INHOMOGENEITIES OF THE THORAX

The solutions of bioelectric forward problems are greatly affected by the model geometries and inhomogeneities. The computational load depends on the resolution of the model and the number of applied inhomogeneities. The effects of geometries and inhomogeneities on simulations have been studied to determine how detailed the models should be in order to incorporate satisfactory forward and inverse solutions.

The effects of inhomogeneities on ECG forward problems have been studied as early as the 1960s when Selvester's group reported that lungs included in the torso model did not change the surface ECG map considerably (Selvester *et al.* 1968). Since then many studies

have been conducted with models containing a number of inhomogeneities including lungs, fat, muscles, blood cavities and bones. The blood cavities, lungs, subcutaneous fat and skeletal muscles have been reported to have rather major influences on bioelectric fields although there is no consensus among the authors as to the most important inhomogeneity (Rudy and Plonsey 1979; Gulrajani and Mailloux 1983; van Oosterom and Huiskamp 1989; Bruder *et al.* 1994; Klepfer *et al.* 1997; Bradley *et al.* 2000; Geneser *et al.* 2008).

Many studies have concluded that the inhomogeneities, in general, affect the magnitudes of torso potentials but not the distribution or pattern of torso potentials (Rudy and Plonsey 1979; Gulrajani and Mailloux 1983; Bradley *et al.* 2000). For example, lungs have been reported to augment the potentials while skeletal muscles attenuate them (Rudy and Plonsey 1979; Gulrajani and Mailloux 1983).

The minor effect of the lungs reported by Selvester *et al.* (1968) was also confirmed by other studies (Rudy and Plonsey 1979; Gulrajani and Mailloux 1983; van Oosterom and Huiskamp 1989; Bruder *et al.* 1994). In contrast, Klepfer *et al*. (1997) found that the lungs have major effect of on surface potentials. Recent studies have recommended that the lungs should be included in torso models because they have a strong influence on epicardial potentials (Bradley *et al.* 2000; Buist and Pullan 2003).

Van Oosterom and Huiskamp (1989) reported that blood cavities and inhomogeneities of torso boundary affect the shape and magnitudes of simulated QRS waveforms. The effect of highly conducting ventricular cavities is also known as the Brody effect (Brody 1956). Bruder *et al*. (1994) have also recommended that ventricular cavities should be included in torso models.

Several studies have recommended that the skeletal muscles should be included in the torso models (Rudy and Plonsey 1979; Gulrajani and Mailloux 1983; Klepfer *et al.* 1997). Bradley *et al.* (2000) have shown that skeletal muscle is less important than previously believed. Instead the subcutaneous fat has been reported to have notable effects on torso potentials and thus it should also be included in models (Klepfer *et al.* 1997; Bradley *et al.* 2000)

Klepfer *et al*. (1997) simulated time-dependent cardiac activity and have reported that the influence of different inhomogeneities also depends on source distribution. The same dependency on source locations has also been reported by other studies (Gulrajani and Mailloux 1983; Bradley *et al.* 2000) .

The sensitivity distributions discussed in this thesis are related to the voltage gradients. The voltage gradients in LV due to the transthoracic and transveneous defibrillation have been reported to be significantly sensitive to the conductivity of the myocardium and less sensitive to other inhomogeneities (Jorgenson *et al.* 1995). Karlon *et al*. (1994) reported that the ribs have only minor effects while other inhomogeneities (including lungs, liver, sternum) have a considerable effect on myocardial current distributions in the case of defibrillation, i.e. sensitivity distribution in the case of ECG measurement.

Most of the studies have been conducted with single geometry although the shape of the volume conductor affects the outcome of forward and inverse solutions. Studies with multiple patient-specific geometries confirm that the shape of torso boundary and different organs, especially ventricular cavities, have a substantial effect on the outcome of forward and inverse solutions (Walker and Kilpatrick 1987; van Oosterom and Huiskamp 1989). Bradley *et al*. (2000) have reported considerable changes in body surface potential magnitudes and patterns due to the heart transitions and rotation. The importance of the relationship between heart and torso geometries on torso potentials have also been reported by other studies (MacLeod *et al.* 1998; Ramanathan and Rudy 2001a).

In contrast to the studies above, Ramanathan and Rudy (2001a; 2001b) have reported the effects of torso inhomogeneities on forward and inverse electrocardiographic simulations to be only minimal. Unlike other reported studies, which in general have applied single dipoles or an otherwise simplified presentation of cardiac activation, Ramanathan applied measured epicardial potentials in forward simulation. The thorax models were based on the VHM and the study also contained simulations with scaled and female thoraxes. The authors conclude that in most forward simulations the thorax can be treated as homogenous. Nevertheless, they propose that the shapes of the thorax and heart as well as their relative position should always be accurately determined with patient-specific models in order to obtain accurate solutions.

In addition to tissue type, the conductivities of different inhomogeneities affect the electric fields. In the literature different values for tissue characteristics such as conductivity, have been given (Rush *et al.* 1963; Geddes and Baker 1967; Foster and Schwan 1989; Gabriel *et al.* 1996a; Gabriel *et al.* 1996c; 1996b). The conductivity values have been reported to have a major effect on surface potentials although the potential distribution patterns were found to be insensitive to individual conductivity values (Bradley *et al.* 2000). Thus valid conductivities are important when accurate anatomical models are applied in bioelectric studies (Hyttinen *et al.* 1997; Bradley *et al.* 2000).

ANISOTROPY OF THE THORAX

Different tissue types, especially muscles, have different electrical properties, conduction velocity and conductivity, with respect to fiber orientation (Rush *et al.* 1963). This anisotropic nature of tissues affects the propagation of electric currents in muscles and thus has an influence on forward and inverse solutions. The anisotropy cannot be applied in models as easily as other tissue properties because fiber orientations cannot be measured *in vivo* or they are not visible in conventional MRI, although diffusion tensor MRI (DTMRI) can provide this information. Typically, the orientations applied to produce anisotropy are from mammals which are mapped to human anatomy (Ramon *et al.* 2000; Wang *et al.* 2001) or computationally approximated (Wei *et al.* 1995).

Different anisotropy ratios for skeletal muscle have been reported in the literature (Burger and van 1961; Rush *et al.* 1963; Epstein and Foster 1983). Myocardial and skeletal anisotropy as well as anisotropy ratio has been found to affect the forward simulations,

BSPM and torso current densities (Karlon *et al.* 1994; Klepfer *et al.* 1997; Ramon *et al.* 2000; Ramon *et al.* 2002; Buist and Pullan 2003). In contrast isotropic heart models have also been shown to give satisfactory results in simple simulations where cell dynamics are not involved (Wei *et al.* 1995).

The effects of anisotropies on sensitivity distributions have not so far been investigated. Various groups have studied the effects anisotropy on defibrillation fields. De Jongh and colleagues (1997) and Eason and colleagues (1998) have analysed the effects of myocardial anisotropy on transvenous defibrillation fields and Seitz *et al*. (2008) studied the effects of skeletal and myocardial anisotropy on defibrillation fields. These studies conclude that anisotropy has only a minor influence on the topology of voltage gradients within the myocardium. Also Wang *et al*. (2001) have shown that myocardial anisotropy has only a minor influence on these voltage gradients.

INHOMOGENEITIES OF THE HEAD

The number of inhomogeneities applied in head models varies. The typical analytical models contain three or four spherical layers representing brain, cerebrospinal fluid (CSF), skull and scalp (Rush and Driscoll 1969; Malmivuo *et al.* 1997). The realistically shaped models represent geometries in more detail and tissue type, such as white matter and grey matter and even separate skull layers (Haueisen *et al.* 1997; Laarne *et al.* 2000; Kybartaite *et al.* 2006). The details of the model increase the computational complexity and load thus making the calculations more time consuming.

The tissue conductivities and head geometry have been reported to have noticeable or even a marked effect on sensitivity distributions of EEG measurements as well as on EEG source localization accuracy (Cuffin 1996; Huiskamp *et al.* 1999; Laarne *et al.* 1999). Ramon and colleagues (Ramon *et al.* 2006) note that a highly heterogeneous model is needed to achieve accurate simulations of scalp potentials. Thus accurate forward modeling requires accurate representation of head geometry and conductivities, at least in clinical situations when patient-specific data is applied.

Spherical models provide an effective means to study electric fields in volume conductor (Rush and Driscoll 1969; Cuffin 1991). Widely-applied three layer spherical head models represent scalp, skull and brain. The electric field magnitudes and topography are affected by the conductivity ratios between these three tissues. Different resistivity ratios have been introduced in different studies. Early studies applied a 1/80/1 resistivity ratio based on Rush and Driscoll's studies with the human skull, *in vivo* data from monkey brain and from the head surface (Rush and Driscoll 1968; 1969). Recently this ratio has been stated to be unrealistic by several authors. Oostendorp and colleagues (2000) reported a ratio of 1/15/1 in their study with *in vivo* and *in vitro* measurements. Other ratios have also been reported during recent years, e.g. 1/8/1 and 1/25/1. (Hoekema *et al.* 2003; Lai *et al.* 2005).

Skull resistivity has a major effect on electric fields. With lower skull resistivity more volume currents flow into the skull from surrounding tissues thus changing the electric

fields (Haueisen *et al.* 1997). This effect is called the shunting effect (Rudy *et al.* 1979). The shunting effect plays a major role in sensitivity distributions of EEG measurements while higher maximum sensitivities are obtained with lower skull/scalp resistivity ratios. Skull resistivity has been reported to influence the spatial resolution and the amount of noise EEG measurements can contain, further affecting the selection of an optimal electrode system (Malmivuo and Suihko 2004; Ryynänen *et al.* 2006).

In general the three layer models do not take into account the well-conducting CSF. The CSF has a substantial effect on the forward and inverse simulations, while resistivity of CSF is lower than in the brain and thus currents will follow the structural paths of CSF in the brain (Ramon *et al.* 2006). The same phenomena of CSF affect EEG sensitivity distributions and thus it should be added as a fourth layer in analytical solutions (Malmivuo *et al.* 1997; Ramon *et al.* 2006; Wendel *et al.* 2008).

Haueisen *et al.* (1997) investigated the influence of tissue conductivities on EEG forward solution with realistic head model containing 13 tissue types. They reported that the surface potentials are sensitive to conductivities of all tissues close to sources and electrodes (i.e. scalp, fat, bone, soft bone, CSF, gray and white matter). In their study tissue characteristics were found to mainly affect strength of potentials and have only minor effects on topology of potential field.

ANISOTROPY OF THE HEAD

The influence of brain tissue anisotropy on EEG has also been reported by several studies (Haueisen *et al.* 2002; Hallez *et al.* 2005; Wolters *et al.* 2006). Haueisen *et al*. (2002) simulated EEG with a single cortical dipole with a realistic FEM model. As in their previous study (Haueisen *et al.* 1997), here they also found that anisotropy mainly affects the strength of potentials and has only a minor effect on the topology of the surface potential field. The results show that the volume current topology inside the volume conductor may vary although the surface potential topology is not greatly affected. The authors also concluded that these anisotropies are not expected to significantly influence EEG source localization accuracy.

Hallez and colleagues (2005) adopted a five layer spherical model in their study of anisotropic brain tissues. The model incorporated skull and white matter anisotropy. The results of the study show that these two anisotropies have a substantial effect on source localization accuracy and should be included in the models. These findings were also confirmed by Wolters *et al.* (Wolters *et al.* 2006) in their study of the effects of anisotropy with realistic head models.

3.2.3 Finite difference method

Numerical element methods have been applied to represent Poisson's equations in volume conductor models as a partial differential format. The present thesis applies the finite difference method (FDM). The literature contains detailed descriptions of different numerical elements, including finite element (FEM) and boundary element methods in

biomedical applications (Johnson 1997; Sachse 2004; Pullan *et al.* 2005). The major difference between FDM and FEM methods is in meshing of the geometry (Pruis *et al.* 1993; Sachse 2004). In FDM there is no need for element-wise interpolation of the solution function. The uniform rectangular grid for FDM is easily adopted, e.g. with segmented images, while meshing of geometry for FEM requires more computational work. Although the geometry is easily converted to a rectangular FDM grid, it is not as effective at describing tissue boundaries as the FEM method because of the "stiffness" of grid. In FDM the solutions are at nodes while in FEM the solutions are interpolated to non-uniform elements between nodes.

In the FDM the segmented volume data is divided into cubic elements forming a resistive network. The data can be originating from MRI which is already in voxel-based format and thus easily adaptable to FDM. The conductivities of the elements correspond to the tissue properties and the dimensions of the elements correspond to the resolution of the image dataset. The network can be described as a set of partial differential equations (PDEs) which present the potentials and currents in each node of the model. The nodes can be positioned either on the corners of the voxel (corner-voxel FDM) or in the centre of the voxel (centre-voxel FDM). The FDM allows the straightforward implementation of complex anatomic geometries from the image data, and the resulting potentials and currents can be calculated within the whole volume conductor model. Different computational implementations for isotropic and anisotropic FDM solutions have been published. (Kauppinen *et al.* 1999a; Takano 2002; Hallez *et al.* 2005; Jing *et al.* 2005; Bruno *et al.* 2006; Barnes *et al.* 2008).

The accuracy of numerical methods has a major influence on the results of the solutions The electric fields solved with FDM have been compared to analytical solutions and it has been noticed that they provide high accuracy although the grid resolution has a major influence on accuracy. Lemieux and colleagues (Lemieux *et al.* 1996) report mean relative errors of 4.2%-9.3% for 1 mm - 1.5 mm grid spacing when comparing spherical FDM to analytical solutions. Gordon and colleagues (Gordon *et al.* 2006) have compared the accuracy of different FDM grids in a homogenous spherical model to the analytical solution. Their study shows that FDM grid resolution has the highest effect on the surface of the model while inside the model difference in potentials due to grid spacing is minimal. The same study shows that the centre-voxel FDM method is slightly more accurate than the corner-voxel at nodes close to the surface of the model.

The linear equations generated on the basis of the FDM grid are solved using iterative methods. The applicability of FDM also depends on these solvers. Several studies have reported on the performance of different solvers based on successive over-relaxation (SOR), conjugate gradient (CG), conjugate gradient preconditioned by symmetric successive over-relaxation (PCG) and algebraic multigrid (AMG)(Mohr and Vanrumste 2003). The AMG was found to be superior over other methods with models containing approximately 70 000 and 550 000 nodes. The amount of arithmetic work employed with AMG was not influenced by the resolution of the model. In a more recent study, geometric multigrid preconditioned CG (GMG-CG) was reported to be even faster and require less memory load than AMG solvers (Barnes *et al.* 2008).

Many studies have applied the FDM in simulations and in the analysis of bioelectric measurements and phenomena. The FDM has been applied in the development of aimed leads for ischemia diagnosis (Hyttinen 1994), analysis unipolar and bipolar ECG leads (Puurtinen *et al.* 2003; Puurtinen *et al.* 2004; Puurtinen *et al.* 2009b), analysis of EEG measurements (Laarne *et al.* 2000; Vanrumste *et al.* 2001; Hallez *et al.* 2005; Jing *et al.* 2005), bioimpedance measurements (Kauppinen *et al.* 1999b; Yang and Patterson 2008) as well as in analysis of cardiac defibrillation (Patterson and Wang 1992; Malik *et al.* 1997).

3.2.4 Lead field and reciprocity

In bioelectric studies there is a need to understand the origin of the measured signal, e.g. ECG or EEG, and investigate the properties of the bioelectric source. As described earlier, the heart-vector represents the electrical activity of the heart. At the beginning of the 20th century Einthoven tried to formulate the relationship between this heart vector and potentials by his limb leads. In his formulation Einthoven presented the heart vector as a two-dimensional dipole at a fixed location (Einthoven *et al.* 1913; Geselowitz 1989). In the mid 1940s Burger and van Milaan described the relationship between a three dimensional heart vector and measured lead potential, V_{lead}, with a lead vector in the following way:

$$V_{LEAD} = aX + bY + cZ = \boldsymbol{c} \cdot \boldsymbol{p} = |\boldsymbol{c}||\boldsymbol{p}| \cos\alpha, \qquad (2)$$

where X, Y and Z are the rectangular components of heart vector, *p*, and a, b and c are the coefficient of the lead vector, *c*. The coefficients of the lead vector depend on the location of the measurement lead, the shape of the volume conductor, the distribution of the inhomogeneities within the volume conductor and the location of the source. They do not depend on the properties of the heart vector. The heart vector can be replaced by any bioelectric source vector and the potential at the lead is a scalar product between lead vector *c* and source vector *p* as illustrated in Figure 3.4a. (Burger and Van Milaan 1946; 1947; 1948)

The source volume can be described with more than a single dipole and thus McFee and Johnston (1953; 1954b; 1954a) extended the lead vector concept to describe the relationship between multiple sources and measured potential. Due to the principle of superposition, the lead potential is the sum of the scalar products of lead vectors and source vectors at each source location:

$$V_{LEAD} = \sum_i \boldsymbol{c_i} \cdot \boldsymbol{p_i}, \qquad (3)$$

where i is the source location within the volume conductor. The combination of lead vectors is called a lead field. The lead field is also considered as the sensitivity distribution of a measurement. Sensitivity distributions can be applied to determine which part of the source volume is actually being investigated with the measurement setup at hand. The lead vector theorem can be applied to any bioelectric source, not only on heart.

Various formulations of lead fields have been introduced. Plonsey expressed the lead field as a potential gradient distribution $\nabla\Phi(\boldsymbol{y})$ and Malmivuo and Plonsey (1995) considered

the lead field as a lead current density distribution $\boldsymbol{J_{LE}(y)}$ as shown in Equations (4) and (5), respectively.

$$V_{LEAD}(\boldsymbol{x}) = \int_H -\nabla\Phi(\boldsymbol{y};\boldsymbol{x}) \cdot \mathbf{J}_i(\boldsymbol{y}) dH, \quad (4)$$

$$V_{LEAD}(\boldsymbol{x}) = \int_H \frac{1}{\boldsymbol{\sigma(y)}} \mathbf{J}_{LE}(\boldsymbol{y};\boldsymbol{x}) \cdot \mathbf{J}_i(\boldsymbol{y}) dH, \quad (5)$$

$$V_{LEAD}(\boldsymbol{x}) = \int_H \frac{1}{\boldsymbol{\sigma(y)}} |\mathbf{J}_{LE}(\boldsymbol{y};\boldsymbol{x})||\mathbf{J}_i(\boldsymbol{y})| \cos\alpha \, dH, \quad (6)$$

where $V_{LEAD}(x)$ is the voltage (e.g. measured ECG or EEG voltage), in lead x, H is the volume conductor, y is a location within H, $\boldsymbol{J_{LE}(y;x)}\left[\frac{\mathbf{1}}{\boldsymbol{cm^2}}\right]$ is the lead vector of lead x in source location y, $\boldsymbol{J_i(y)}\left[\frac{\boldsymbol{A}}{\boldsymbol{cm^2}}\right]$ is the impressed source current density vector in source location y, $\boldsymbol{\sigma}(y)\left[\frac{\mathbf{1}}{\boldsymbol{\Omega cm}}\right]$ is the conductivity tensor at the source location in the volume conductor and $\boldsymbol{\alpha}$ is the angle between heart vector and lead vector.

RECIPROCITY THEOREM

The lead field in the volume conductor can be established by applying Helmholtz's reciprocity theorem (Helmholtz 1853; Malmivuo and Plonsey 1995). In short, the reciprocity theorem states that it is possible to swap location of source and detector without any resulting changes in signal amplitude.

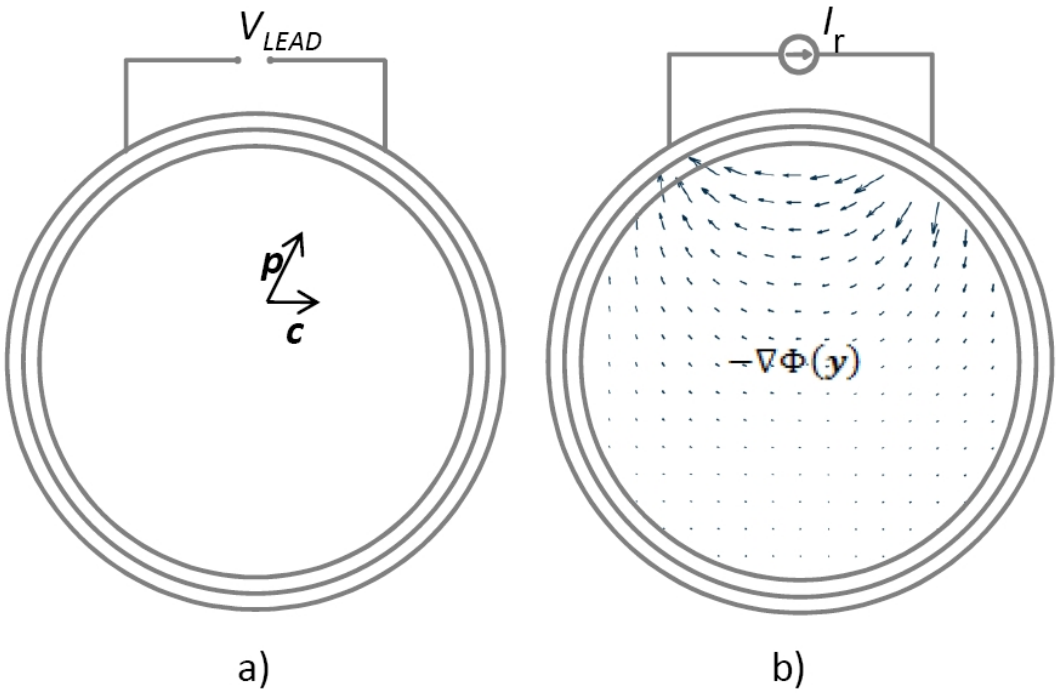

Figure 3.4 Lead field and reciprocity theorems. a) The lead voltage V_{lead} is affected by lead vector *c* and source vector *p*. b) The reciprocal current I_r gives rise to a potential gradient field $\nabla\Phi(\boldsymbol{y})$, which is the lead field.

The lead field can be established by introducing a reciprocal current I_r to the measurement electrodes which raises the potential gradient distribution, $\nabla\Phi(\boldsymbol{y})$, i.e. lead field to the volume conductor (Equation (7) and Figure 3.4b) (Plonsey 1963).

$$-\nabla \cdot (\boldsymbol{\sigma}(\boldsymbol{y})\nabla\Phi(\boldsymbol{y})) = \begin{cases} I_r\,, & in\ electrodes \\ 0\,, & elsewhere \end{cases} \qquad (7)$$

The lead field $\boldsymbol{J}_{LE}(\boldsymbol{y})$, as defined in (5) and (Malmivuo and Plonsey 1995), is calculated from gradients of Φ(y) as defined in Equation (8) (McFee and Johnston 1953). The essential benefit of the reciprocal method is that the sensitivity of a measurement lead at all source locations in the volume conductor can be determined by means of a single calculation. Thus, when combined with Helmholtz's reciprocity theorem, the lead field theory provides an efficient method to study the sensitivity distributions.

$$\boldsymbol{J}_{\mathrm{LE}}(\boldsymbol{y}) = -\boldsymbol{\sigma}(\boldsymbol{y})\nabla\Phi(\boldsymbol{y}) \qquad (8)$$

ANALYSIS OF SENSITIVITY DISTRIBUTIONS OF BIOELECTRIC MEASUREMENTS

The sensitivity distributions of ECG were first reported by Mcfee and Johnston (1953; 1954b; 1954a). Mcfee and Johnston demonstrated the use of lead fields in analysing ECG leads and constructing optimal measurement field in the heart. Their studies show that measurement signals can be weighted with resistor networks so that optimal field is obtained.

More recent ECG studies have examined sensitivities of bipolar and unipolar leads on different regions of the myocardium as well as the applicability of lead field magnitudes in the evaluation of signal amplitudes (Hyttinen *et al.* 1993; Hyttinen 1994; Puurtinen *et al.* 2009b).

Hyttinen *et al.* (1995) optimized VCG leads and aimed the lead sensitivity on certain regions of the myocardium using a reciprocal lead field approach. They applied a thorax model and lead vectors of a 12-lead ECG system as well as Frank's VECG lead system to detect 15 source dipoles. The group successfully applied the lead field method and produced an optimal VECG system based on a 12-lead ECG that had notably higher (10-20%) orthogonality than Frank's system.

Puurtinen *et al.* (2009b) studied the applicability of the lead field method in estimating ECG amplitudes by comparing sensitivity distributions and clinical data. In the study they compared the average magnitudes of lead fields of 117 unipolar leads with peak-to-peak QRS amplitudes of the same leads. They also constructed 42 precordial bipolar leads. The study contained two different thorax models and QRS data of 236 subjects. The results of the study indicate that the lead field magnitude and QRS-amplitude correlate well in the case of unipolar leads and moderately in the case of bipolar leads.

Rush and Driscoll (1969) applied reciprocal theorem with analytical formulation of a three-layer head model in their analysis of EEG lead sensitivities. The study demonstrates

how lead placement and distance affects the lead field at different depths of the volume conductor.

The sensitivity distributions can also be applied to study the spatial resolution of scalp EEG. Malmivuo *et al.* (1997) and Wendel *et al.* (2008) have introduced the concepts of half-sensitivity volume (HSV) and fifth-sensitivity volume (FSV), respectively. The HSV and FSV concepts describe the volume within the source region in which the magnitude of sensitivity is at least 50 % or 20 % of the maximum, respectively. These measures of sensitivity distribution describe how concentrated the sensitivity distribution of the lead is. The more concentrated the measurement sensitivity is, the better is the spatial resolution.

Using the same approach as Rush and Driscoll, Malmivuo *et al.* (1997) have studied the sensitivity distributions of two- and three-electrode setups. They applied HSV in the analysis. The study shows that with shorter electrode distances (under 60°) both two- and three-electrode setups have smaller HSV. The results also indicate that the three-electrode setup always measures the radial component of cortical sources while the short-distance two-electrode setup measures the tangential component.

The effect of electrode distance and skull resistivity on the EEG spatial resolution has been studied using the lead field approach. Malmivuo and Suihko (2004) reported that the interelectrode distances have less effect on the spatial resolution of EEG when lower and more realistic skull resistivities are applied. The depth of the sensitivity distribution, i.e. the maximum depth of HSV, has been reported to be between 1.8 cm and 3.7 cm, depending on bipolar electrode distance and skull resistivity (Ferree *et al.* 2001).

Wendel *et al.* (2008) have studied the effects of CSF on sensitivity distributions and reported that the highly conducting CSF channels the current. Because of this the maximum sensitivity on cortical structures is decreased. The results of the study suggest that the spherical models should have the CSF as a fourth layer.

The reciprocal lead fields have also been applied in the design of improved lead configurations which are sensitive to deep EEG sources (Väisänen and Malmivuo 2009). These weighted leads have close to uniform sensitivity distributions within the brain volumes in spherical head models. They thus provide better quality signals generated by deep sources than traditional bipolar EEG configurations. The study demonstrates that a uniform lead field within a three-dimensional homogeneous spherical model is obtained when the injected reciprocal current at every electrode is incrementally proportional to $\cos\theta$ and $\cos\phi$. The θ and ϕ are the angular displacements of the electrode from the negative z-axis and xz-plane, respectively. The same cosine proportion was applied by Geselowitz and Arthur (1971) in two-dimensions when they derived aimed ECG leads.

4 MATERIALS AND METHODS

Figure 4.1 presents the modelling approaches applied in the studies of the present thesis. The analytical solution and numerical FDM were used as computational methods in the analysis of bioelectric measurements. This thesis applies a spherical head model and a VHM-based realistically shaped thorax model. The analysis of the measurement setups is based on the analysis of sensitivity distributions induced into the volume conductor by reciprocal unit currents.

The thesis introduces ROISR and sensitivity field analyses in studying the properties of ECG and EEG measurements. The theory behind the ROISR analysis method is presented with a spherical head model. Validation of the method was conducted with spherical head model simulations, high resolution EEG measurements and with ECG BSPM simulations. The specificity of bipolar EEG, unipolar surface ECG and implantable ECG were studied using the ROISR method. The effects of ECG implant dimensions as well as implantation on sensitivity distribution were studied by applying field analysis.

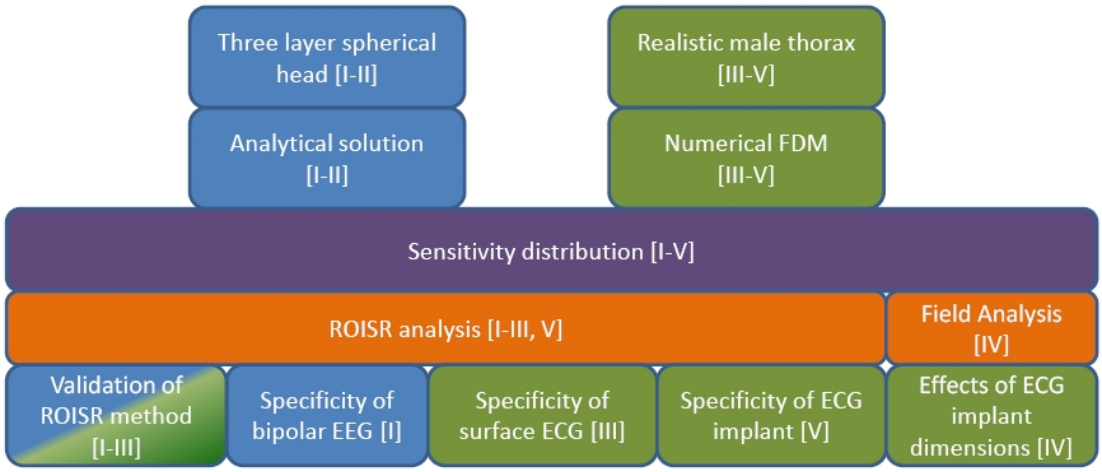

Figure 4.1 Modelling approaches and properties of measurements studied.

4.1 Modelling methods

4.1.1 Volume conductors and FDM

Spherical models provide an effective means for investigating bioelectric phenomena in a volume conductor. Thus the sensitivity distributions of bipolar EEG leads in publications [I] and [II] were solved with an analytical three-layer spherical head model (Rush and Driscoll 1969). The three layers comprise scalp, skull and brain, the radii of the spheres being 92, 85 and 80 mm, respectively. The resolution of the model was 2 mm x 2 mm x 2 mm containing 267 730 nodes. The calculations for the analytical model were executed with Matlab in a desktop computer. As mentioned in Section 3.2.2, various scalp/skull/brain resistivity ratios have been introduced in the literature. Calculations were conducted with a 1/15/1 ratio while Oostendorp *et al.* (2000) concluded that this is a feasible ratio in three layer models if CSF is not present.

An FDM model of the 3D male thorax applied in publications [III]-[V] is based on the VHM data (Ackerman 1991; Kauppinen *et al.* 1998). The size of the model was 250x250x95 with resolution in the slices close to the heart 1.67 mm x 1.67 mm x 4 mm and elsewhere 1.67 mm x 1.67 mm x 8 mm. In total the model contains 2.7 million nodes with 2.6 million elements. The model was isotropic and represents over 20 different organ and tissue types including all the important ones reported in the literature such as the myocardium, ventricular cavities, lungs, skeletal muscle and subcutaneous fat. The resistivities of the tissues are listed in [IV].

The sensitivity distributions in the realistic male thorax were calculated by applying the principle of reciprocity. The current distribution corresponding to the lead field current density was generated into the volume conductor by applying the unit currents to the electrode pairs. The FDM solver was originally developed by Walker and Kilpatrick (1987) and further developed by Hyttinen (1994) and Kauppinen *et al.* (1999a). The present version, applying the Incomplete Cholesky Preconditioner and Conjugate Gradient for solution, has been developed by Takano (2002). The software was executed on an AMD 3000+ 64Bit, 2 GB RAM, 200GB SATA RAID computer. Calculation of a lead field for all the nodes in the 2.6 million element model took approximately 10 to 15 minutes.

4.1.2 Region of interest sensitivity ratio

Previously only a few quantitative parameters, such as HSV, have been applied in the analysis of sensitivity distributions of bioelectric measurements. Thus one of the thesis objectives was to develop novel methods for sensitivity distribution analysis. In the present thesis a parameter called ROISR is developed to characterize how well the sensitivities of different bioelectric measurement leads are concentrated in the ROI compared to other source regions. At first the ROISR was developed for analysis of EEG measurement systems in publications [I] and [II] but it was further applied to analyse ECG systems in publications [III] and [V].

The ROISR defines how much better the measurement setup is to measure signal sources as against unwanted sources. Equation (9) defines ROISR as the ratio between the average sensitivities of a predefined ROI and the rest of the source volume (nonROI). ROISR value 1 means that the measurement is equally specific to activation in the ROI and outside it. The higher the ROISR, the more specific and concentrated, i.e. aimed, the measurement is to the selected ROI and the more likely changes in activation will be seen in the measured signal. The ROISR could thus be interpreted as the specificity of the measurement lead.

$$\mathrm{ROISR} = \frac{\frac{1}{H_{ROI}}\int_{H_{ROI}} G_{ROI}(\boldsymbol{y};\boldsymbol{x})d\boldsymbol{y}}{\frac{1}{H_{nonROI}}\int_{H_{nonROI}} G_{nonROI}(\boldsymbol{y};\boldsymbol{x})d\boldsymbol{y}} \quad , \qquad (9)$$

where G is the magnitude of sensitivity, H_{ROI} is the ROI source volume [cm^3] and H_{nonROI} is the nonROI source volume [cm^3] within the volume conductor.

The sensitivity G applied in ROISR calculations can include only the lead vector magnitude (Equation (10a)) or both magnitude and angle, (α), between lead vector, $\boldsymbol{J}_{LE}(\boldsymbol{y})$, and source vector, $\boldsymbol{J}_i(\boldsymbol{y})$, (Equation (10b)).

$$G(\boldsymbol{y};\boldsymbol{x}) = \begin{cases} \frac{1}{\sigma(y)}|\boldsymbol{J_{LE}}(\boldsymbol{y};\boldsymbol{x})| & (a) \\ \frac{1}{\sigma(y)}|\boldsymbol{J_{LE}}(\boldsymbol{y};\boldsymbol{x})||\cos(\alpha)| & (b) \end{cases} \qquad (10)$$

Equation (10a) for sensitivity G should be applied when the directions of sources cannot be estimated or in cases where the sensitivity distribution is optimally oriented parallel to sources, i.e. cos (α) equals 1. If the directions of sources are known, the sensitivity G should interpreted with Equation (10b).

For example, it has been recognized that measurable EEG potentials are generated by pyramidal neurons of same orientation and the sources are described with equivalent dipoles (Nunez 1981; Niedermeyer and Lopes da Silva 1993). In such cases the direction of the equivalent source within, e.g. visual cortex (the ROI), is known and Equation (10b) can be applied for G_{ROI}. However, spatially random dipoles have been applied as sources generating background EEG, i.e. noise, and thus the direction of the noise sources in the brain (nonROI) are still unknown and Equation (10a) is applied for G_{nonROI} (de Munck *et al*. 1992; Lutkenhöner 1998a; 1998b).

The ROISR was introduced and validated for EEG and ECG lead analysis in publications [I]-[III] and it was applied in publications [III] and [V] to study specificities of surface ECG and implantable ECG measurements, respectively.

4.1.3 Relationship between ROISR and SNR

As the ROISR was designed for EEG measurement analysis it is assumed that the desired signal is generated by the sources within ROI and other sources in the volume conductor

produce unwanted noise to the measured signal. Thus it is assumed that the ROISR parameter has a strong correlation to the SNR of an EEG measurement. Equation (11) describes the SNR of a measurement based on lead vector approach (Equation (6)). Here the wanted signal is raised by sources lying in the ROI and unwanted noise originates from the sources in the nonROI volume.

$$\text{SNR} = \frac{signal}{noise} = \frac{\int_{H_{ROI}} \frac{1}{\sigma} |\boldsymbol{J_{LE}}||\boldsymbol{J_i}| \cos\alpha d\boldsymbol{y}}{\int_{H_{nonROI}} \frac{1}{\sigma} |\boldsymbol{J_{LE}}||\boldsymbol{J_i}| \cos\beta d\boldsymbol{y}} \sim \frac{|\boldsymbol{J_i}| \int_{H_{ROI}} |\boldsymbol{J_{LE}}| d\boldsymbol{y}}{\int_{H_{nonROI}} |\boldsymbol{J_{LE}}| d\boldsymbol{y}}, \quad (11)$$

Equation (11) applies few simplifications to the original SNR equation based on the following assumptions: Firstly, the conductivity σ is reduced from the equation because ROI and nonROI are within e.g. the brain volume having constant conductivity. Secondly, the sources in EEG can be described as equivalent dipoles. It is assumed that the sources within the ROI can be replaced by an equivalent dipole vector J_i, which has constant direction and magnitude (de Munck *et al.* 1988a). It is also assumed that the measurement set up is optimally selected and thus the sources within ROI are parallel to the sensitivities and thus the cos (α) equals 1 in each source location. Thirdly, spatially random dipoles have been applied to model the sources generating background EEG, i.e. noise (de Munck *et al.* 1992; Lutkenhöner 1998a; 1998b). Because the orientations or magnitudes of the random noise source dipoles cannot be estimated accurately, the magnitude of J_i,, within nonROI is approximated to be equal to one. In the worst case the sources within nonROI are parallel to the sensitivities and thus the cos (β) equals 1 in each source location. It can be observed that the ROISR has similar notation (Equation (9)).

4.1.4 Field analysis

Measured signal is affected by the lead vector direction and magnitude as defined in Equation (6). The differences in two measurements and signals due to changes in lead fields within source volumes can be estimated by analysing the relative differences between the magnitudes of the lead fields and how the lead field direction is changed. These differences were studied in publication [IV].

Equation (12) describes how the changes in magnitude and direction of the lead vector at location *y* affect the relative difference of the measured potentials between leads V_1 and V_2.

$$\frac{V_1}{V_2} = \frac{|\boldsymbol{J_{LE}}(\boldsymbol{y};\mathbf{1})||\boldsymbol{J_i}(\boldsymbol{y})||cos(\alpha \pm \beta)|}{|\boldsymbol{J_{LE}}(\boldsymbol{y};\mathbf{2})||\boldsymbol{J_i}(\boldsymbol{y})||cos(\alpha)|} = \frac{|\boldsymbol{J_{LE}}(\boldsymbol{y};\mathbf{1})||cos(\alpha \pm \beta)|}{|\boldsymbol{J_{LE}}(\boldsymbol{y};\mathbf{2})||cos(\alpha)|}, \quad (12)$$

where $|\boldsymbol{J_{LE}}(\boldsymbol{y};\mathbf{1})|$ is the magnitude of lead vector at location *y* for lead 1, $|\boldsymbol{J_{LE}}(\boldsymbol{y};\mathbf{2})|$ is the magnitude of lead vector at location *y* for lead 2, $|\boldsymbol{J_i}(\boldsymbol{y})|$ is the magnitude of source vector at location *y*, α is the angle between source and lead vector in case 1,β is the change in lead vector direction between lead 1 and lead 2

According to Equation (12) the change in lead field magnitude and direction affect to the measured signal when comparing two cases which have the same source distribution. It can also be observed that the relative difference between the magnitudes of lead vectors is directly reflected in the change in measured lead voltage. We can also see that the larger the change in lead vector direction, the larger is its effect on the signal. It is also seen that the effect of change in lead vector direction is dependent on the angle between source and lead vector in lead 1. The analysis is based not only on the average changes within the whole lead field but also on local changes through standard deviations of magnitude and direction changes.

4.2 Validation of ROISR

4.2.1 EEG measurements

The ROISR is assumed to have a connection to the SNR of the same measurement lead. The correlation between ROISR and the SNR of a measurement lead was demonstrated with a visual evoked potential (VEP) experiment [I]. The VEP was selected because the active region within the occipital cortex corresponding to P100 component can be represented with a single ROI. The VEPs were measured with Neuroscan (SynAmp, Neuroscan) and 256-channel EEG cap containing 254 EEG channels and 2 ECG channels. The VEP experiment was based on checkerboard stimulation procedures described in (Celesia *et al.* 1993). The stimulations were made using Stim (Neuroscan). During the experiment 290 evoked responses was measured. The measurements were conducted with two volunteers, male and female, hereafter testee 1 and testee 2, respectively.

The sensitivity distributions and further ROISRs for all 254 measurement leads of both testees were calculated with the analytical three-layer spherical head model. The electrode locations applied in the calculations were digitized during the measurements with FastTrak (Polhemus) and late fitted on the surface of the spherical model. Figure 4.2 presents the numbering and locations of the centre line electrodes of testee 2.

The SNR of each lead was calculated employing methods adopted from (Raz *et al.* 1988). The focus of interest was the P100 component of the VEP response generated on the visual cortex. Because of this the SNRs were calculated for the time interval between 70 and 130 ms after the stimulus in order to avoid other evoked responses generated elsewhere in the brain. For each lead 290 epochs were included in the calculation of SNRs.

A spherical segment of 20 mm radius on the cortex was selected as the ROI by observing anatomical images and previous studies as to the size of the primary visual cortex (Andrews *et al.* 1997). The VEPs are generated on the primary visual cortex which in the spherical model can be approximated to a site under electrodes 130-134, as illustrated in Figure 4.2 (Watson 2000).

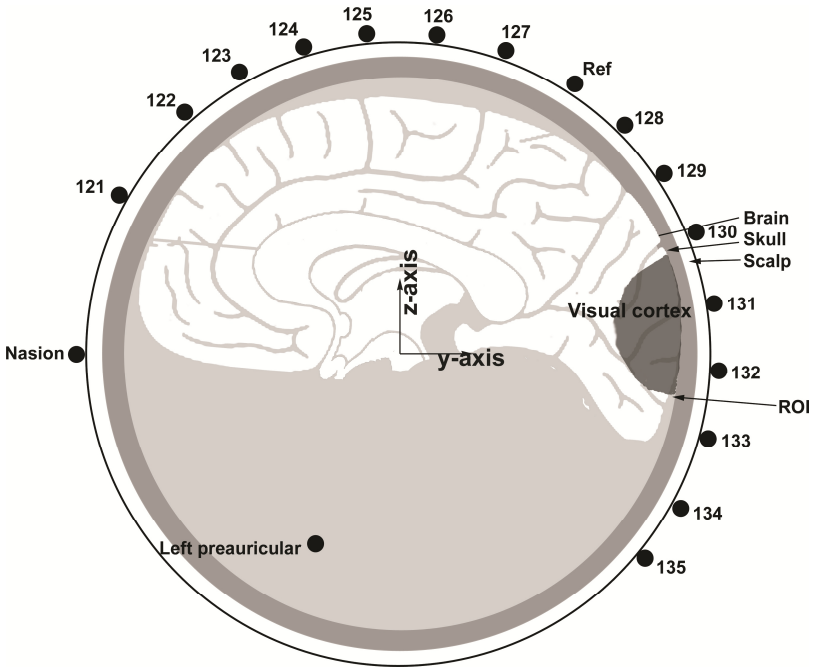

Figure 4.2 Illustration of locations for electrodes 121 to 135 applied in the measurements and fitted on the spherical model. The region of interest is illustrated in dark grey. [I]

In the ROISR it is assumed that signal sources are within the ROI and noise sources outside it and therefore the highest correlations between the ROISRs and SNRs of 254 EEG leads should be achieved when the ROI is located in this region of signal sources. The effect of ROI location on the correlation was studied by locating the ROI under electrodes 121-135 and calculating the ROISRs of the leads in these cases. The correlations were calculated applying three different assumptions of source orientations within ROI; unknown, tangential (+z) and radial (+y).

4.2.2 EEG simulations

The connection between the ROISR and SNR of a measurement lead was also validated with EEG EP simulations [II]. In some EP studies the active region is on the cortex, e.g. in visual evoked potentials, and thus in the simulations the ROI was located at the cortical region shown in Figure 4.3.

The background activity has been modelled with spatially random dipoles and homogeneously distributed random dipoles (de Munck *et al.* 1992; Lutkenhöner 1998a; 1998b). Some studies have proposed that there are local and global systems producing the measured EEG (Nunez 2000). As there is no precise information as to how the noise and signal source distributions in the brain should be modelled and simulated, we investigated a total of 16 cases, 4 different source distribution models with 4 different source orientations, listed in Table 1 were investigated. The aim was to examine how the correlation between ROISR and SNR would be affected by different kinds of source distributions and thus how applicable the ROISR is for estimating the relative SNR of a measurement lead if the distribution in the volume conductor is not precisely known.

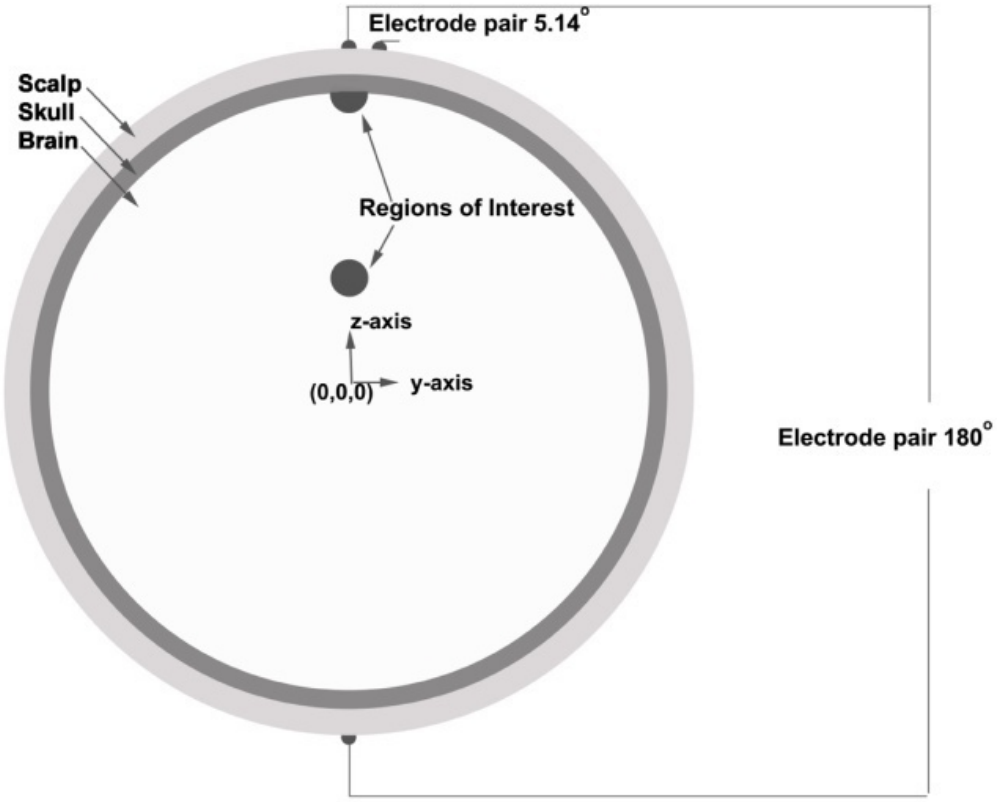

Figure 4.3 Cross-section of the three-layer spherical head model with minimum and maximum electrode distances. The cortical ROI and non-cortical ROI located within the brain are indicated with dark grey circles. [I]

Table 1 The four models and source orientations producing the 16 cases simulated. Source distribution models: Sources in all or random locations within ROI and nonROI volumes. Source orientation models for sources within ROI: Optimal, sources in directions of sensitivities. Random, sources in random directions. Sources in positive tangential and radial directions (Figure 4.3) .

		Source Distributions			
Source Orientations		ROI, all nonROI, all	ROI, all nonROI, random	ROI, random nonROI, all	ROI, random nonROI, random
	Optimal	Case 1.1	Case 2.1	Case 3.1	Case 4.1
	Random	Case 1.2	Case 2.2	Case 3.2	Case 4.2
	Tangential (+y)	Case 1.3	Case 2.3	Case 3.3	Case 4.3
	Radial (+z)	Case 1.4	Case 2.4	Case 3.4	Case 4.4

The EEG was simulated with a three-layer spherical head model. The simulated EEG signal $V_{LEAD}(t)$ contains evoked signal components at time t, $V_{signal}(t)$ and random noise components $V_{noise}(t)$ as described in Equation (13). In the brain region there may be either equivalent signal source or noise source vectors. Each signal source vector in the model has the magnitude of a modified sine wave and the direction is dependent on the case studied. The modified sine wave simulated an activation sequence which also involved consecutive time instants with zero amplitude. In each case studied the noise sources had random magnitudes and directions. Each signal simulating an evoked potential epoch contained 44 samples (t =44).

The EEG signals produced by sources within the ROI were simulated by calculating the lead fields for 35 bipolar EEG leads and multiplying the lead field matrices, J_{LE}, by the source distribution matrices, J_i (Equation (14)). The bipolar leads had interelectrode distances of between 180 degrees and 5.14 degrees. For all the 16 cases we simulated signals of 138 epochs for all 35 different leads.

$$V_{LEAD}(t) = V_{signal}(t) + V_{noise}(t), \qquad (13)$$

$$V_{signal}(t) = \frac{1}{\sigma}\sum_k \mathbf{J}_{LE,k} \cdot \mathbf{J}_{i,k}(t), \qquad (14)$$

where $V_{LEAD}(t)$ is the total signal in a lead, V_{signal} (t) is the signal produced by sources of interest, k are the locations of signal sources within the ROI, $J_{LE,k}$ is the lead vector in location k, is the source vector in location k, and t is the sample number between 1 and 44.

The simulated responses also contain abundant noise and thus some averaging of the repeated epochs is normally applied to reveal the actual signal of interest. The amount of noise decreases when the epochs are averaged, and the SNR increases as a result. The method introduced by Raz and colleagues (1988) was applied in calculating the SNRs of the averaged epochs.

The correlation coefficient between the ROISRs and SNRs of the 35 leads with different numbers of averaged epochs were calculated for all the 16 cases.

4.2.3 ECG simulations

In order to validate the ROISR method with the ECG measurements the ROISR maps of 117 leads where compared to the BSPMs simulated with uniform epicardial dipolar distributions [III]. The ROISR values were calculated for 117 leads of a Dalhousie body surface ECG mapping system (Montague *et al.* 1981) that is presented in Figure 4.4. The LV was divided according to the standard 12 segment LV subdivision recommended by the Committee on Nomenclature of Myocardial Wall Segments of the International Society of Computerized Electrocardiography (Figure 4.4) (Wagner *et al.* 1984; Startt/Selvester *et al.* 1989). The ROI and nonROI volumes in the ROISR calculations were such that the epicardial surface of each corresponding segment was the ROI while the rest of the ventricular epicardial surface, including right ventricle, was the nonROI volume.

Surface potentials, $V_{LEAD}(x)$, were simulated at each 117 measurement lead by assigning dipoles, $\boldsymbol{J}_i(\boldsymbol{y})$, with a direction normal to the epicardial surface over the entire ventricular epicardium. The sensitivities of leads to different myocardial segments, i.e. ROIs, were tested by suppressing the dipolar sources within the selected region and solving the lead potentials. The effects of the suppressed ROI sources on the potentials were observed by calculating the potential differences to the reference case. In the reference case all sources were active. The body surface potential difference maps show if the changes in lead potentials are recognizable and which leads are specific to the absence of the sources in a specific ROI.

4.3 Analysis of bipolar EEG measurements with ROISR

The effects of electrode separation on the specificities of bipolar EEG leads were analyzed with ROISR [I]. The study contained 70 bipolar EEG leads with interelectrode distances

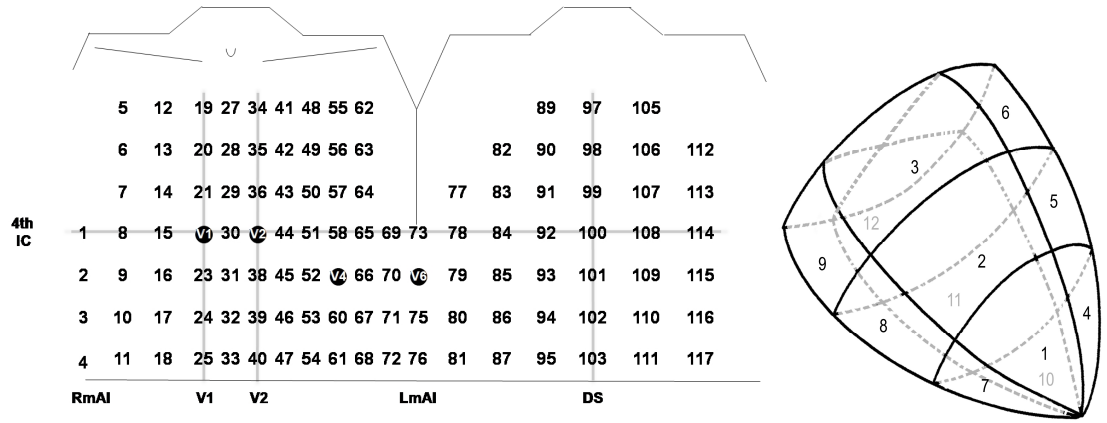

Figure 4.4 Dalhousie lead system (left) and 12 segments of left ventricle (right).

from 180 degrees to 2.57 degrees. The effect of ROI location on the specificities of bipolar leads was also studied and thus two different ROIs were applied, one lying on the cortex and the other deeper in the brain [I]. Both ROIs were spherical volumes with a 20 mm radius. The coordinates for the centre of the ROI lying on the cortex were x=0 mm, y=0 mm and z=80 mm and for the deeper ROI x=0 mm, y=0 mm and z=30 mm. Figure 4.3 presents two bipolar electrode pairs with the 5.14° and 180° electrode distances applied in this study, and the locations of the ROIs in the brain in a 2D yz-plane. The effects of electrode distance were studied employing three different assumptions about the source orientation within the ROI. The ROISRs were calculated with unknown source orientation by applying Equation (10a) and with known source orientation by applying Equation (10b). For simplicity the known source orientations were selected to be radial (+z) and tangential (+y) directions.

4.4 Analysis of body surface ECG measurements with ROISR

The specificities of the 117 leads of a Dalhousie lead system to different segments of the LV myocardium and the entire right ventricular free wall were analyzed in publication [III]. The ROISRs of the 117 lead system were calculated for all 12 individual LV segments as described in Section 4.2.3.

In addition the specificity of leads to three larger ROI volumes was studied. In the case of infarction the leads having specific sensitivity to the infarcted section should reveal the absence of sources while in a normal case it should show their presence. Thus the specificity of the leads to larger myocardial volumes such as the right ventricular free wall (RV) and the myocardium related to anterior and inferior infarctions was also studied. The anterior infarction volume contains the myocardium supplied by the left descending artery or its branches (segments 1-7, 10 and 11) and the inferior infarction volume contains the myocardium supplied by the inferior descending artery or its proximate coronary (segments 8 and 9) (Startt/Selvester *et al.* 1989). The ROISRs for the anterior and inferior ROIs were calculated by applying the corresponding segments as ROI and the remaining ventricular epicardium as the nonROI volume. Altogether the specificities of leads to 15 different ROI volumes were studied.

In order to study the effect of source direction estimation on the ROISR both Equation (10a) and (10b) were applied for sensitivities. The sources vectors directed normal to the epicardial surface were implemented as a definition of the equivalent source directions (α).

4.5 Analysis of implantable ECG measurements

4.5.1 Effects of implant dimensions on ECG measurement sensitivity

Implantation of any measurement or stimulating device into the human body is an invasive, time-consuming, expensive and almost irreversible operation. The effects of implantation or implant design on the measurement cannot thus be tested and reviewed

by actually implanting the device into humans during the design process. To achieve successful measurements by implanted devices it is vital to have knowledge of the effects of the implantation or implant design on the measurements. There is thus a need for methods providing such information without the actual implantation of a device in test subjects, and such information would be most valuable if available already during the design process. The lead field method affords an effective means of investigating characteristics such as implant dimensions and implant location on measurement sensitivity distributions within the myocardium.

The effects of change in an implant's width, thickness and length (i.e. electrode distance) on measurement sensitivity were studied in publication [IV]. The dimensional combinations tested are listed in Table 2. The implant model had electrodes attached to the ends. The implant was located vertically on the left side of the thorax model described in Section 4.1.1 and to follow the contours of the body surface. The location of the implant is in the region between precordial leads V3 and V4 of the standard 12-lead ECG system. The electrodes were approximately 5 mm under the body surface. Figure 4.5 illustrates the model of the thorax with the implant.

The biocompatible coating materials applied in the implants, e.g. parylene, epoxy or silicon have high resistivities and therefore a non-conducting implant body was modelled with a resistivity of 10^{10} Ωcm, which corresponds to the resistivity of the air in the model.

The effects of dimensional changes to the relative differences in magnitude and direction were studied by means of sensitivity distribution field analysis presented in Section 4.1.3. The sensitivity distributions within the myocardium were calculated by inducing reciprocal unit currents to the electrodes. The effects of dimensions were also studied without the implant insulated body in the model.

4.5.2 Effects of electrode implantation on ECG measurement sensitivity

Vertical bipolar electrode pairs were implanted at three depths as shown in Figure 4.6 in order to study the effects of electrode implantation on the ECG measurement [IV]. The electrode pairs were located on the body surface, under the fat and under the skeletal muscle, the implantation depths below the body surface being 16.67 and 33.34 mm, respectively. The relative differences in magnitude and direction were studied with sensitivity distribution field analysis as presented in Section 4.1.3. The sensitivities of the implanted pairs were compared with that of an electrode pair on the body surface.

Table 2 Dimensions of the tested ECG implant designs for reference implant and smaller implants whose one dimension is changed. The changed dimension indicated in bold.

	Dimensional Combinations (mm)					
	Reference implant	**Case1**	**Case 2**	**Case 3**	**Case 4**	**Case 5**
X	6.67	**3.33**	6.67	6.67	6.67	6.67
Y	23.38	23.38	**9.99**	**3.33**	23.38	23.38
Z	60	60	60	60	**40**	**20**

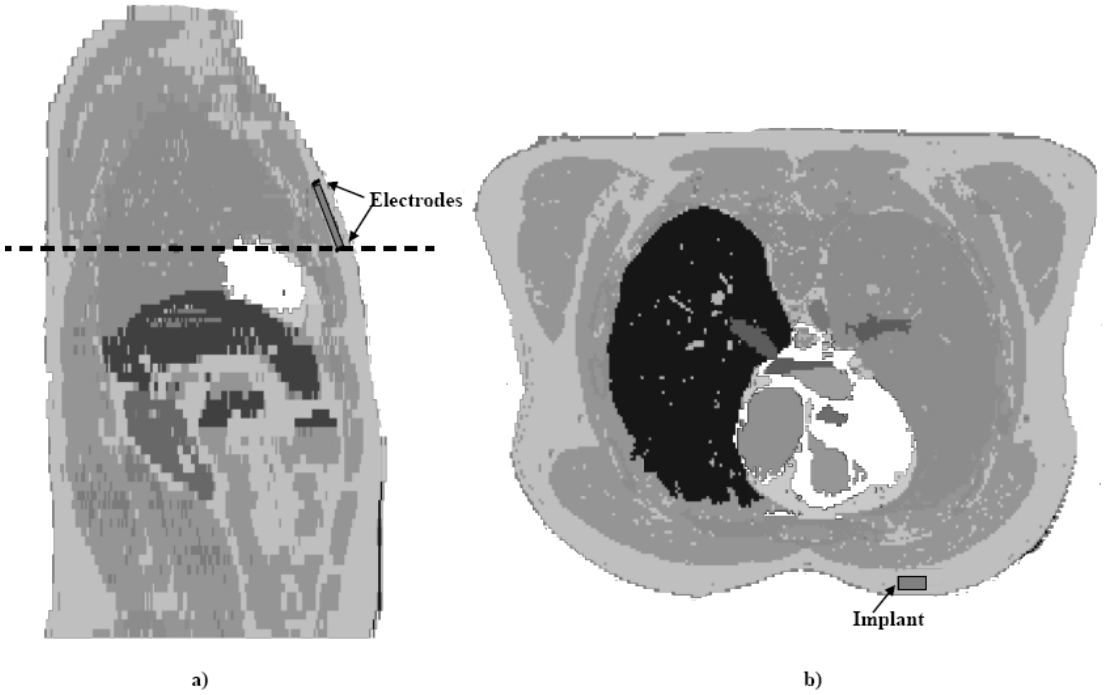

Figure 4.5 The sagittal (a) and transverse (b) illustrations of the model with implant inside. In (A) the electrodes illustrated in black and the heart muscle in white. The transverse illustration is from the slice marked with dot line.

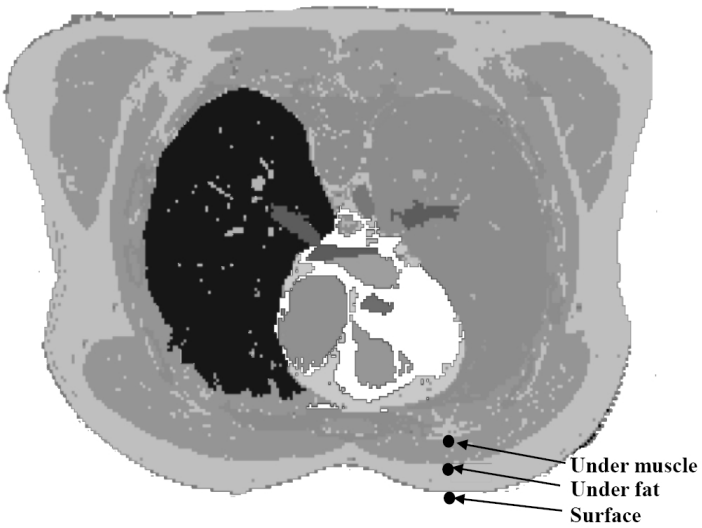

Figure 4.6 Locations for lower electrodes on body surface, under fat and under muscle.

4.5.3 Effects of implantation site on ECG measurement specificity

The ROISR method was applied when the specificity of an implantable ECG to different segments of the LV myocardium was being studied [V]. The objective was to evaluate the effects of implantation location on the specificity of the measurement. The ROISRs were calculated for cases where the implant was in a vertical orientation, at 6 different locations in the upper thorax illustrated in black in Figure 4.7. The depth of implantation in each case was approximately 5 mm below the body surface corresponding to implantation under the skin. The LV was divided into 12 areas representing possible regions of interests as described in Section 4.2.3. The ROISRs for all the 12 segments were calculated in such way that one segment was ROI and the other areas in the left ventricle where treated as nonROI source areas. The same procedure was applied for all six implant locations. The ROISRs were calculated with unknown source directions and thus the Equation (10a) was applied.

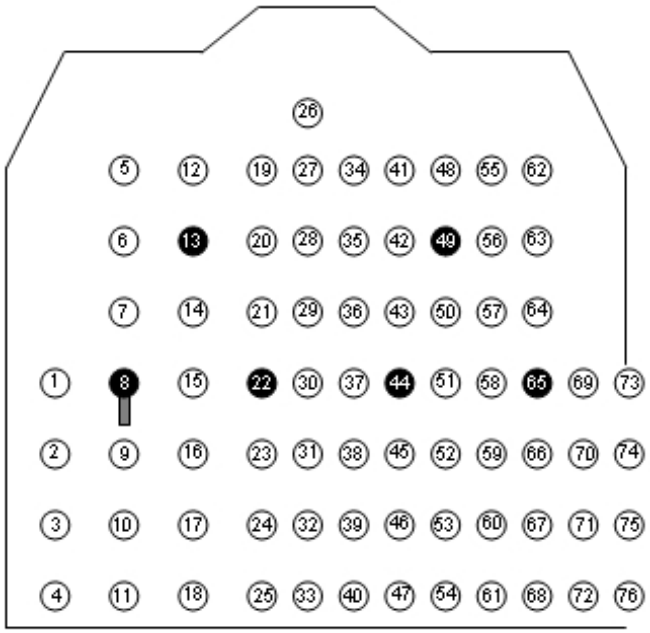

Figure 4.7 Locations for ECG implants. Numbering of the locations according to the Dalhousie system [V].

5 RESULTS

5.1 Validation of ROISR

5.1.1 EEG measurements

The correlation between the ROISR parameter developed here and the SNR of the measurement lead was demonstrated using preliminary VEP measurements in publication [I]. The effect of the ROI location on the correlation was tested with the measured VEP data as described in Section 4.2.1. The ROI location was varied under electrodes 121-135 (Figure 4.2). Figure 5.1a presents the correlations between ROISRs and SNRs of 254 EEG leads as a function ROI location with an unknown source direction in the ROISR calculation. The ROISR and SNR have higher correlations (> 75%) when the ROI is located under electrodes 131-134, where the visual cortex is located, but very low for other ROI locations. When the ROI was located within the occipital lobe (under electrode 131) the correlations between ROISR and SNR for testees 1 and 2 were 82% and 94%, respectively.

The effect of the assumption of source direction was also tested using VEP data. Figure 5.1b shows that if the sources are assumed to be in a positive radial-direction, high correlations between the ROISR and SNR are achieved for the same ROI locations as in Figure 5.1a when the source directions were assumed unknown. As Figure 5.1c shows, the correlations are notably lower when the sources are assumed to be in a positive tangential-direction. These results imply that the sources producing P100 component in the primary visual cortex are most likely to be radially oriented.

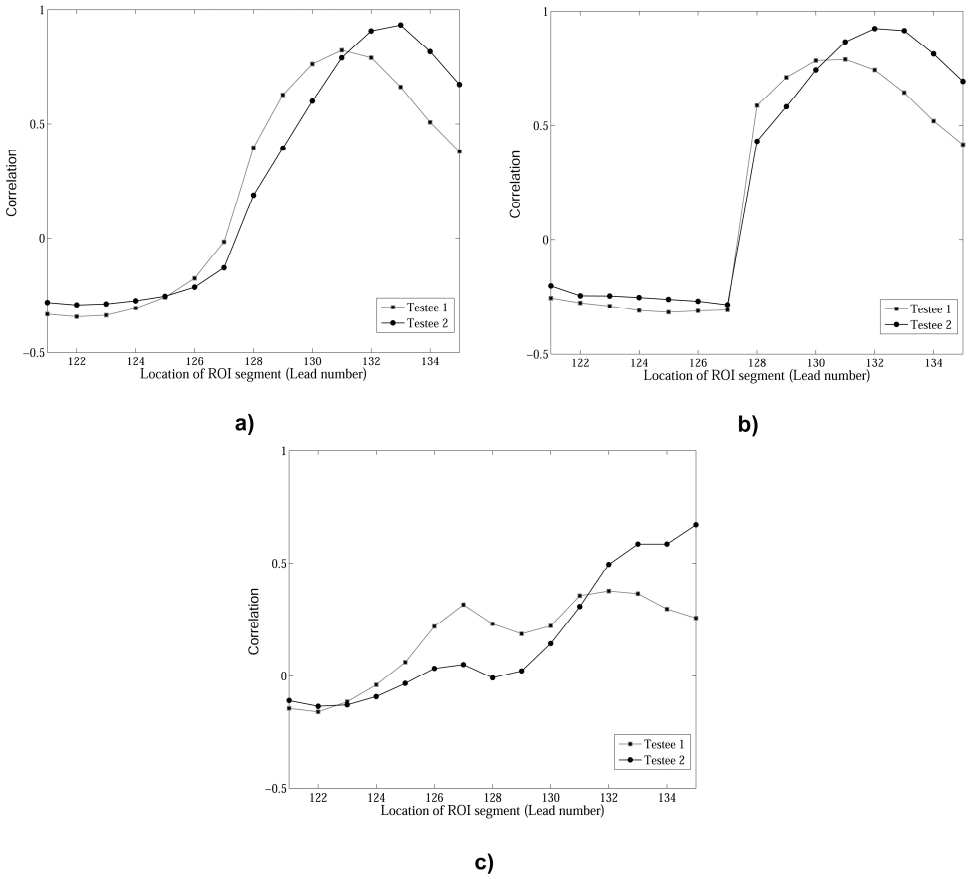

Figure 5.1 Correlation between ROISR and SNR as a function of ROI location (Figure 4.2) when orientation of sources is assumed to be unknown (a), radial (b) and tangential (c).[I]

5.1.2 EEG simulations

The preliminary EEG measurements showed a strong correlation between the ROISR and SNR of a measurement lead. In the ROISR it is assumed that noise sources are outside the ROI but there is no precise information as to how the noise and signal source are distributed within the brain. Publication [II] investigated how the correlation between ROISR and SNR would be affected by different kinds of source distributions within the brain.

The EEG-evoked responses were simulated with 16 cases describing four source orientation and four source distribution models as described in Section 4.2.2. Figure 5.2 presents examples of simulated signals for case 1.3 when sources within ROI were tangentially oriented. The example shows that the measurement becomes more specific to the tangential sources when electrode separation decreases. Because of this the ROISR and the SNR of the measurement are increased.

Table 3 presents the average correlations for all 16 cases when 1 to 138 epochs were averaged. The overall results show that the correlation between ROISR and SNR was good

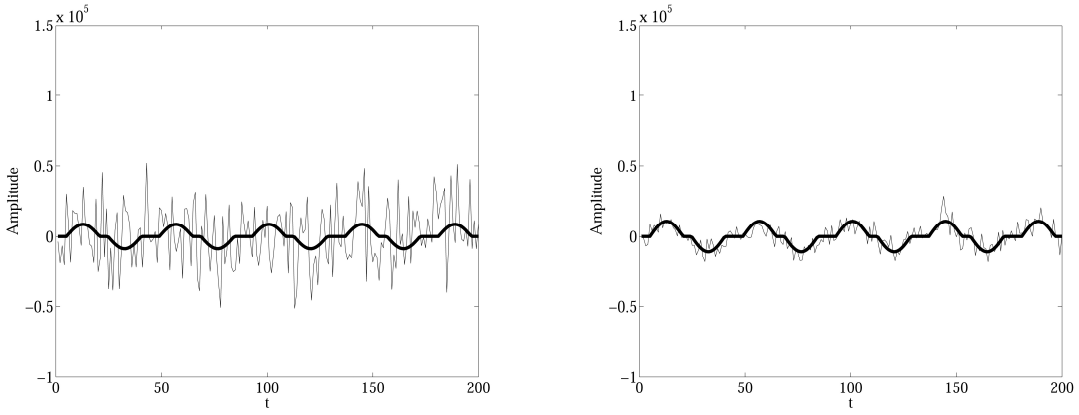

Figure 5.2 Examples of simulated signals (grey) for case 1.3 with electrode separations 30.8° (a) and 5.14° (b). The signals produced by sources within the ROI are presented with black. The $ROISR_{tan}$ are 3.30 (a) and 19.10(b). The SNRs are 0.27 (a) and 1.30(b).

Table 3 Average correlations between SNRs and ROISRs of 35 leads in different simulated cases when 1 to 138 epochs were averaged.

		Average Correlations							
		Case 1.1	Case 1.2	Case 1.3	Case 1.4	Case 2.1	Case 2.2	Case 2.3	Case 2.4
SNR vs.	ROISR	0.99	0.71	0.86	0.74	0.99	0.49	0.86	0.76
	$ROISR_{tan}$	1.00	0.80	0.95	0.55	1.00	0.61	0.95	0.59
	$ROISR_{rad}$	0.79	0.36	0.51	0.97	0.78	0.08	0.51	0.98
		Case 3.1	Case 3.2	Case 3.3	Case 3.4	Case 4.1	Case 4.2	Case 4.3	Case 4.4
	ROISR	0.98	0.92	0.87	0.68	0.97	0.79	0.87	0.67
	$ROISR_{tan}$	1.00	0.93	0.96	0.50	0.96	0.69	0.96	0.48
	$ROISR_{rad}$	0.78	0.71	0.54	0.93	0.81	0.84	0.54	0.93

for all source distribution models. $ROISR_{tan}$ and $ROISR_{rad}$ were calculated by applying corresponding source directions when the magnitudes of sensitivities were calculated with Equation (10b). The correlations are also high in cases where the sources are randomly distributed within ROI and nonROI volumes, cases 4.x.

The results of the preliminary measurement showed that higher correlations are achieved when the source directions are correctly applied in ROISR calculations. The same results are confirmed by the simulations. For example in case 1.3 the ROI sources are tangential

and the correlation with ROISR, $ROISR_{tan}$ and $ROIRS_{rad}$ are 0.85, 0.95 and 0.51, respectively. Both measurements and simulations also show that correlations are high even if the source directions are assumed unknown. The highest correlations are achieved if the sensitivity distribution is optimally oriented.

The correlation is poorest in cases where the signal sources lie in random directions (cases x.2) within the ROI, but such cases are not realistic because measurable EEG potentials are generated by pyramidal neurons of the same orientation (Niedermeyer and Lopes da Silva 1993).

5.1.3 ECG simulations

In order to validate the ROISR method with ECG the BSPMs were simulated with uniform epicardial dipole distributions [III]. The ROISR maps and potential difference maps were calculated with methods described in 4.2.3. Figure 5.3 presents examples of ROISR and potential difference maps when the ROI was the RV free wall, the anterior LV and the inferior LV. The differences in lead potentials when sources in specific segments are suppressed mimic e.g. infarcted areas. Suppressing sources in anterior segments causes the potentials on the left mid-thoracic region to increase by over 40 and thus these leads are most specific to present the changes in activation on these segments. In comparison, suppressing sources in RV has only a minor effect on the potentials at the leads. By comparing the ROISR maps to the potential difference maps it is clearly seen that the highest ROISR values are located in the same areas as the highest positive potential changes.

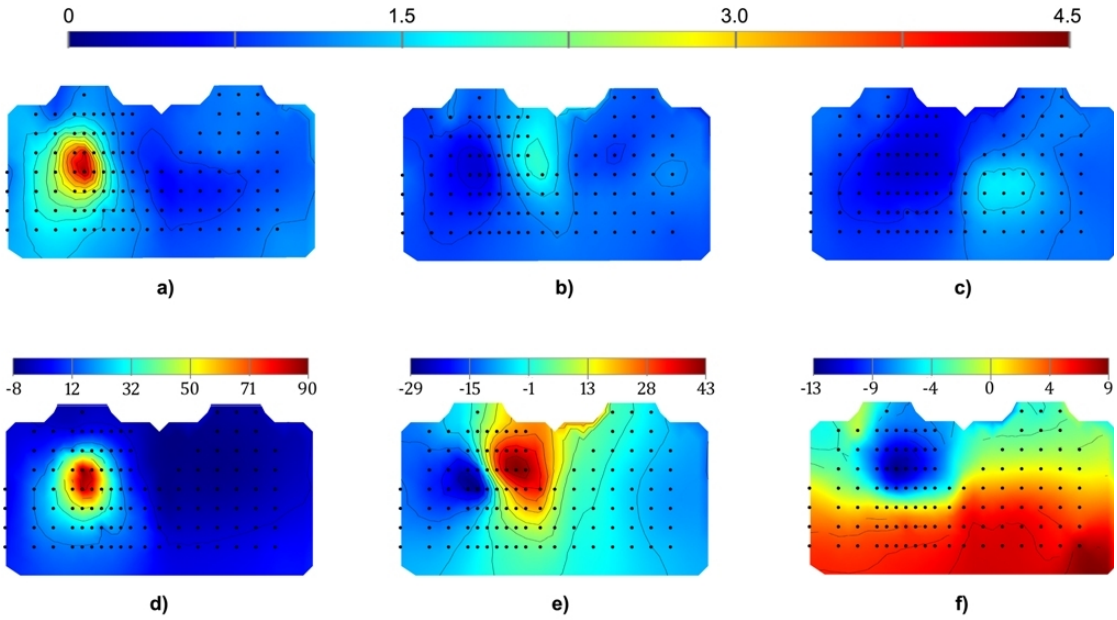

Figure 5.3 ROISR (a,b,c) and potential difference (d,e,f) maps with RV free wall (a,d), Anterior segments (b,e) and Inferior segments (c,f) as ROI.

5.2 Specificity of bipolar EEG leads

Figure 5.4 presents the directions and normalized magnitudes of sensitivities for electrode separation of 5.14° (A) and 180° (B) on the yz-plane. Figure 5.5 presents the ROISRs for a cortical ROI (A) and a non-cortical ROI (B) as a function of the electrode separation. Figure 5.5 also presents the sensitivity ratios in cases where the sources are supposed to be in the tangential or radial directions within the ROI: these sensitivity ratios are here called as $ROISR_{tan}$ and $ROISR_{rad}$, respectively.

From Figure 5.4a it can be seen that with 5.14° electrode separation the sensitivity is high within the cortical region while in the other regions it is close to zero. Figure 5.4 also shows that the sensitivities within the cortical ROI are mostly oriented tangentially along the y-direction with 5.14° separation and radially along the z-direction with 180° separation. This is reflected in the values of the $ROISR_{tan}$ and $ROISR_{rad}$ presented in Figure 5.5a. It can be observed that in the case of cortical ROI when decreasing electrode separation the measurement becomes more specific to the sources directed in either tangentially or radially but with short enough separation the specificity to the sources in radial direction begins to decrease. This is also demonstrated with the simulated signals presented in Figure 5.2.

Figure 5.5b presents the ROISRs of non-cortical ROI as a function of electrode distance. The behaviours of the ROISR, $ROISR_{tan}$ and $ROISR_{rad}$ are seen to differ slightly from Figure 5.5a. The $ROISR_{tan}$ starts to rise rapidly when separation is decreased and the $ROISR_{rad}$ does not increase as the separation is reduced but instead, it starts to decrease with electrode separations shorter than 100°.

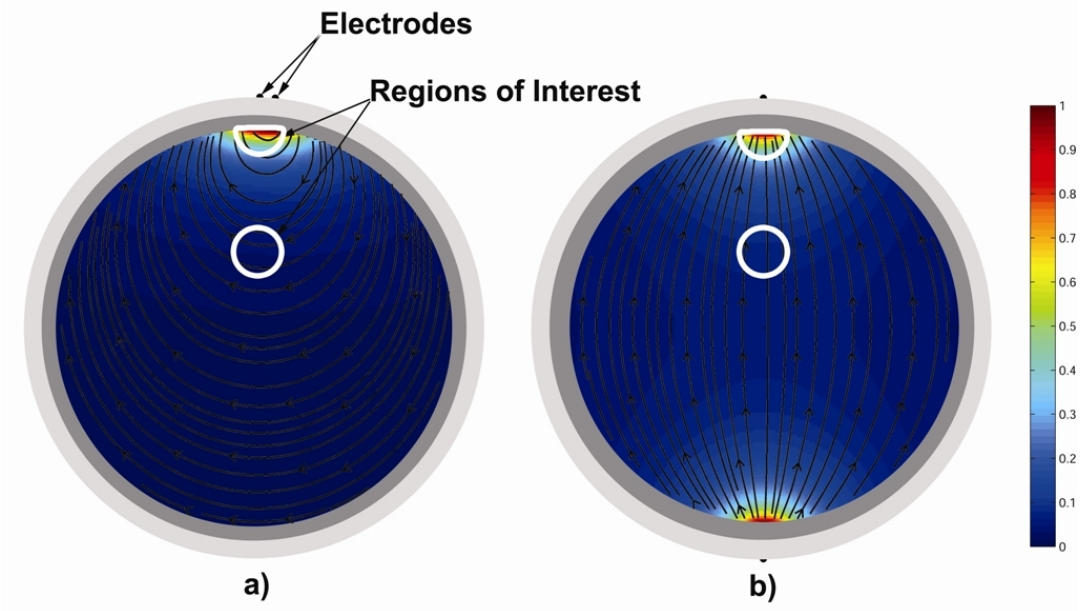

Figure 5.4 Normalized magnitudes of sensitivity for leads with minimum (a) and maximum (b) electrode distances in plane y=0. Cortical ROI and deeper ROI are shown in white.

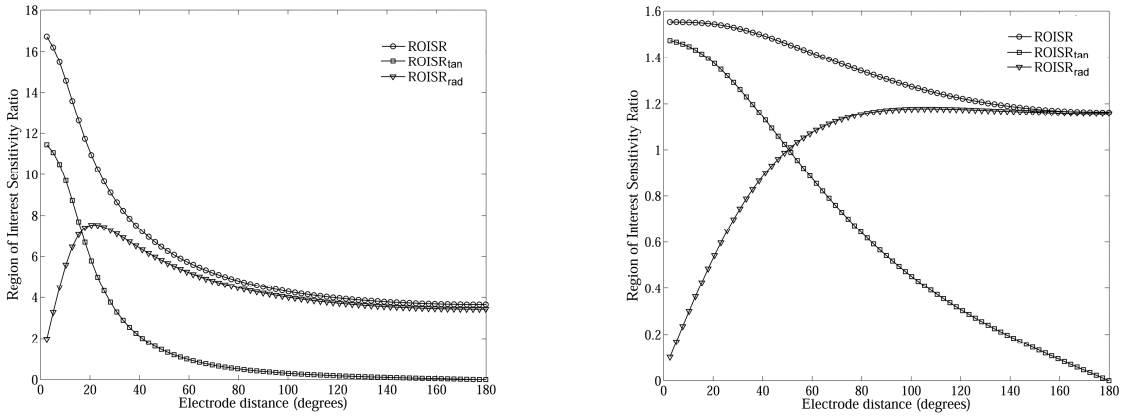

Figure 5.5 ROISR, $ROISR_{tan}$ and $ROISR_{rad}$ as a function of electrode separation when the interest of measurement is on the sources within cortical ROI (A) and non-cortical ROI (B).

5.3 Specificity of body surface ECG leads

Figure 5.6 presents the ROISR maps when ROI is one of the 12 segments in the left ventricle. Here the source directions are considered to be unknown and Equation (10a) is applied as sensitivity G in Equation (9). The ROI is one of the 12 segments in the LV. On the basis of the ROISR maps half of the segments (1, 4, 5, 10, 11 and 12) have leads which are expected to be clearly specific on the ROI sources. These segments have leads with over 2.25 ROISR values. Some of the segments (6,7,8 and 9) have leads with ROISR values over 1.5 and thus these are expected to be slightly specific to the ROI. Only septal segments 2 and 3 do not have leads which are expected to be clearly specific to them.

As expected, the left mid-thoracic region have leads which are specific to anterior segments (1, 4, 5), leads on the posterior site are specific to posterior segments (10-12). Highly specific leads to detect the right ventricular free wall are located around leads V1 and V2 (Figure 5.3). The optimal leads for detecting changes in ECG caused in the LV anterior myocardium are located in the upper left thoracic area around Lead 64 (Figure 5.3).

Figure 5.7 presents the ROISR maps when the source directions are assumed to be normal to the epicardial surface. By comparing Figure 5.5 and 5.6 it can be seen that there is little effect on the ROISRs or specific leads between the cases when the source directions are known or unknown in ROISR calculations.

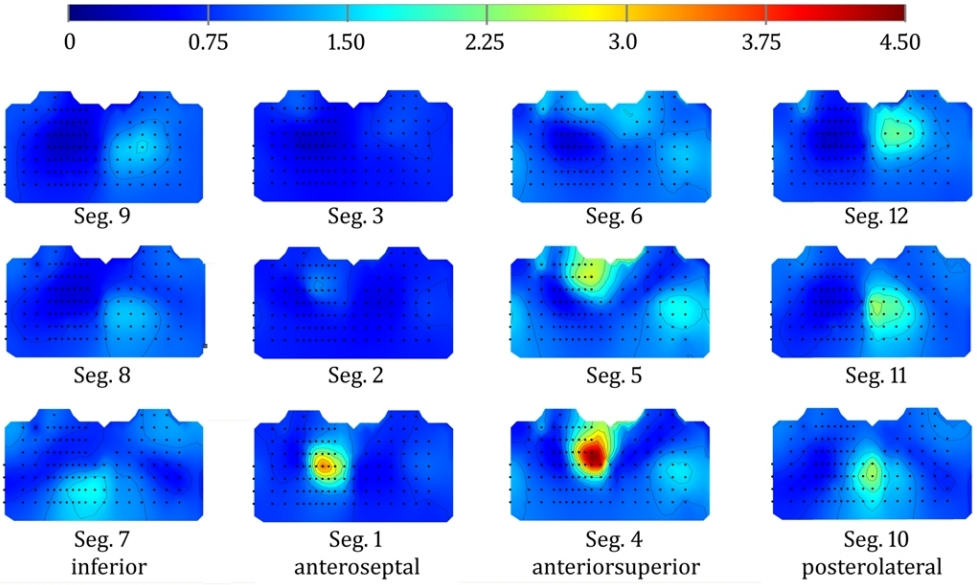

Figure 5.6 Body surface ROISR maps with corresponding segment (1-12) as ROI. Here the source directions are assumed to be unknown. Value 1 means that the measurement is equally specific to the activation within the ROI and outside it.

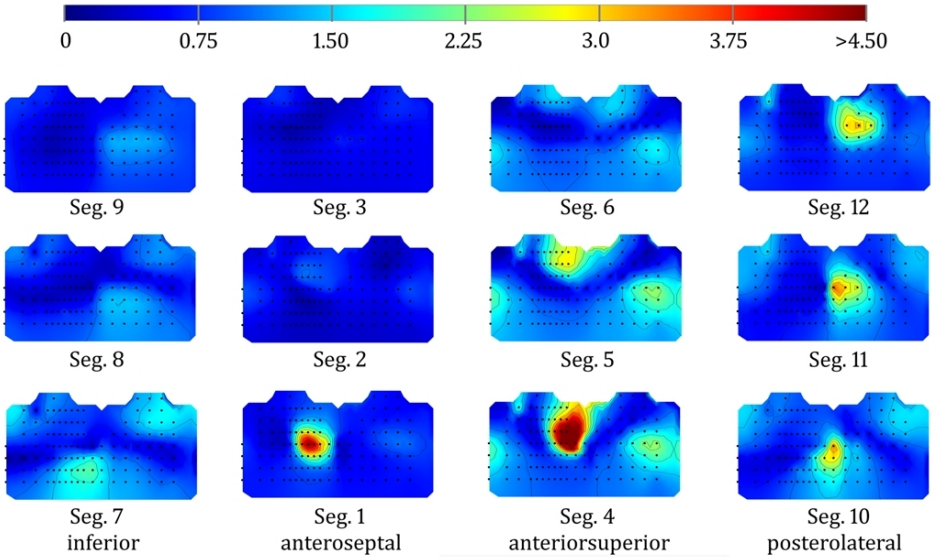

Figure 5.7 Body surface ROISR maps with corresponding segment (1-12) as ROI. Here the source directions are assumed to be normal to epicardial surface. Value 1 means that the measurement is equally specific to the activation within the ROI and outside it.

5.4 Implantable ECG measurements

5.4.1 Effects of implant dimensions

The effects of implant dimensions on sensitivity distributions were analysed employing the methods presented in Section 4.5.1. The average changes in magnitude and direction of the lead field within the heart muscle are presented in Table 4 [IV]. The direction change corresponds to β in Equation (11). The findings illustrate the obvious fact that interelectrode distance has a major effect on measurement sensitivity compared to the other dimensions of the implant. This finding became evident, for example, when the width of the implant was reduced from 23.38 mm to 9.99 mm; the resulting average magnitude of the lead field decreased by only 3.2 % and direction was changed by 1.9 degrees, while reducing the implant interelectrode distance relatively less (from 60 mm to 40 mm) reduced the average magnitude by 34.7 % and direction changed by 2.5 degrees.

Publication [IV] also examined the effect of the physical non-conductive implant between the electrodes on the measurement sensitivity in the heart muscle. It was shown that when there is no non-conducting implant between the electrodes, the average magnitude of sensitivity on the heart muscle is 5-12% lower than in the cases where there is non-conducting medium between electrodes.

The effects of implantation depth on the average magnitude and direction of the lead field in the heart muscle were studied in publication [IV]. The findings indicate that the average magnitude of the sensitivity is increased by 13.32 and 29.45 when the electrodes are being implanted under the fat and muscle, respectively. It is worth noting that although the average is increased, a more important change is seen in the behaviour of the standard deviation of the magnitude change. The standard deviation of changes in these cases is quite large (11.00 and 32.84, under fat and muscle, respectively) compared, for example, to cases where implant dimensions are altered, to a maximum of 6.8 (Table 4). The larger standard deviation would imply larger local variation between changes in lead vector magnitudes. Figure 5.8 illustrates the local changes in sensitivity magnitude in

Table 4 Effects of dimension change. Average changes in lead vector angle and magnitude when one dimension at a time is changed.

	Thickness (x)	Width (y)		Length (z)	
	Case 1	Case 2	Case 3	Case 4	Case 5
ΔDirection (°)	0.3	1.9	3.4	2.5	5.9
Std ±	0.2	1.5	1.9	1.5	3.4
ΔMagnitude (%)	-3.7	3.2	4.1	-34.7	-69.1
Std ±	2.5	4.3	6.6	6.8	3.8

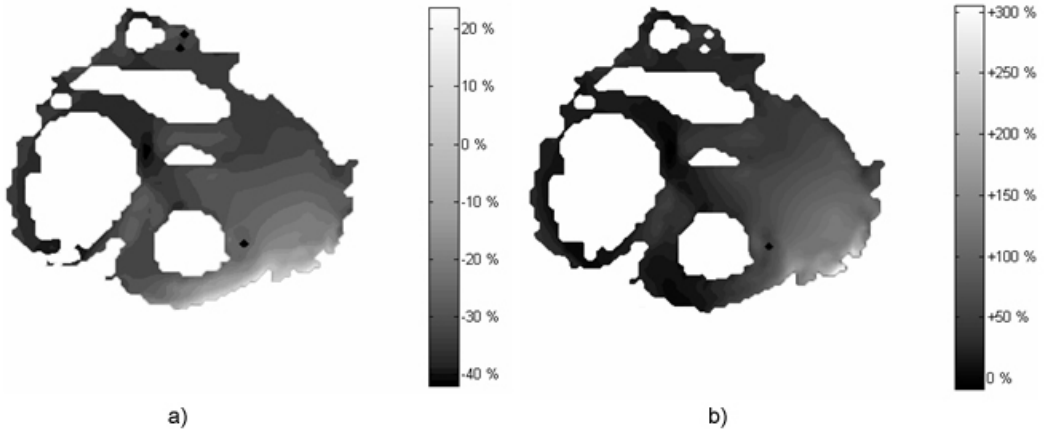

Figure 5.8 The change in local sensitivity magnitude within the myocardium at transverse level presented in Figure 4.5. (A) implant length is reduced from 60 mm to 40 mm. (B) electrodes are implanted under the muscle.

the transverse plane, for the cases where implant length is reduced from 60 mm to 40 mm (A) and when electrodes are implanted under the muscle (B). It can be observed in Figure 5.8 that the effects of electrode implantation are more significant on local measurement sensitivities than the effects of electrode distance. Implantation might, therefore, have a major effect on the morphology of the measured signal

5.4.2 Effects of implant location on specificity

As shown with EEG and ECG simulations, the ROISR method provides an effective means to investigate the specificity of lead configurations. The implantable ECG devices could be applied specifically to monitor activation of a particular myocardial segment. As shown with ECG simulations, different lead locations are specific to different myocardial segments. Thus in publication [V], ROISR was applied to investigate specificity of six implantation sites on LV segments.

Table 5 presents the ROISRs for six implant locations when one of the 12 segments of LV is the ROI and the other source areas in the LV are nonROI areas [V]. The higher the ROISR is, the more concentrated the measurement is on the selected ROI and it is more likely that the changes in activation are seen in the measured signal.

For example, one may be interested to measure and monitor changes in the activation of segment 4 and thus the measurement needs to be specific to this region. From this it can be observed that location 65 has the highest ROISR for segment 4. On average this measurement site is 3.74 times more sensitive to the changes in activation of the sources in 4th segment than to the changes in activation of other source locations in the LV.

Table 5 ROISRs for 12 different ROI segments with 6 different implant locations and vertical alignment. If the ROISR is >1 then the measurement is, on average, more specific to the measurement sources within ROI than the sources outside it.

	Vertical orientation											
	Number of ROI Segment											
	Anteroseptal			Anterosuperior			Inferior			Posterolateral		
Locat.	1	2	3	4	5	6	7	8	9	10	11	12
8	0.83	0.69	0.68	0.86	0.89	0.86	1.29	1.15	0.91	1.34	1.46	1.34
13	0.84	0.80	0.74	1.13	1.44	1.47	0.82	0.79	0.77	0.87	0.99	1.41
22	1.13	0.64	0.49	2.45	1.22	0.66	1.23	0.69	0.45	2.38	1.17	0.64
44	1.69	0.70	0.41	3.19	0.98	0.49	1.47	0.64	0.35	2.39	0.91	0.48
49	1.08	1.01	0.84	1.66	2.16	1.37	0.76	0.62	0.48	0.81	0.78	0.79
65	2.37	0.92	0.47	3.74	0.99	0.43	1.32	0.58	0.32	1.76	0.60	0.37

Another possible way to interpret the results is to predict where the changes in signal have originated. For instance, if there are changes occurring in the measured signal when the implant is located at location 44, the ROISR could tell how probable it is that changes are originating in each segment. In this case the highest ROISR (3.19) is in segment 4 and the second highest (2.39) is in segment 10. In this case if there are changes in the measured signal, they would most probably be generated in the area of segments 4 or 10.

6 DISCUSSION

The sensitivity of an ideal measurement should focus more intensively on selected target areas compared to other source areas of the volume conductor, thus yielding more specific measurements. The purpose of the thesis was to develop a quantitative method for the analysis of this sensitivity contrast between different source regions. Further, this method could be applied to evaluate the relative SNR of bioelectric measurements by means of modelling and applied, for example, when new patient-specific aimed measurement setups are being designed.

6.1 Applicability of ROISR in analysing bioelectric measurements

In this thesis the ROISR method was been developed to describe the specificity of a bioelectric measurement. Preliminary EEG measurements showed that ROISR has a high correlation (82% and 94%) with the SNR of the measurement. The theoretical relationship between ROISR and SNR of EEG measurement is shown in Section 4.1.3. The straight correlation between ROISR and SNR is achieved with certain boundary conditions: 1) all the sources within the ROI have the same direction and magnitude, 2) the background activity is generated by spatially random dipoles. The first assumption is considered to be valid because it has been stated that the large group of neurons having the same direction produce measurable potentials and further equivalent dipoles can be applied to describe cortical generators (Nunez 1981; de Munck *et al.* 1988a). However the assumptions applied do not take into account temporal changes in activity.

In addition to the previous assumptions the ROISR method is based on the average sensitivities within the signal source volume and noise source volume. In an ideal case the ROI and nonROI volumes are selected in such a way that they are full of signal and noise sources, respectively. Based on principle of superposition, the signal and noise are produced by all active sources within the corresponding volumes. In such an ideal case

the sum of sensitivities would be applicable instead of the average of sensitivities when ROISR is calculated. In a realistic case, however, the ROI cannot be selected to be such that it is full of signal sources and contain only these sources of interest. Furthermore, the noise sources often have random behaviour and locations in the case of EEG. The average of sensitivities is thought to take into account these uncertainties in the selection of ROI and nonROI volumes.

In practice the ROI is not full of signal sources and may even contain noise sources. Source directions can also vary within the ROI. The preliminary EEG measurements also showed that the assumption of source direction has a marked effect on the correlation between ROISR and SNR. Because of this the EEG simulations in this thesis were applied to study how much the above mentioned assumptions of source direction and distribution affect the correlation between ROISR and SNR and applicability of ROISR in analysing EEG measurements.

In the case of ECG similar assumptions are not valid because the "noise" sources are not random and the activation in different regions of the myocardium is also often simultaneous. Thus the selection of ROI and nonROI sources is more complicated when considering which parts of the myocardium are signal sources and which noise sources. The separation of signals generated by sources of interest and other myocardial activation is also rather complicated. Thus, instead of describing SNR of measurement in the case of ECG, the ROISR can be considered solely to determine how well-aimed the measurement is. In the thesis ECG simulations were applied in order to study the applicability of ROISR in analysing this specificity of the ECG measurement leads.

6.1.1 Effect of ROI in EEG measurement

In this thesis the preliminary 254-channel VEP measurements of two testees were applied to study the correlation between ROISR and SNR of the EEG lead [I]. The ROISRs were shown to have substantially high correlations with the SNRs obtained from real VEP measurements. The correlations were high (82% and 94% for both testees) when the ROI was selected from the occipital lobe. With other tested ROI volumes located outside the occipital lobe the correlations were very poor (<50%). Thus the selection of ROI is critical when applied in the analysis of measurement leads. High correlations were also reported by Sinkkilä in her Master of Science thesis in which there was a total of 14 VEP measurements from 7 patients. Ten of 14 measurements had correlations over 90% and only 2 had correlations under 75% (Sinkkilä 2010).

One of the assumptions when ROISR was being developed was that ROI covers only signal sources. The effect of this assumption on the accuracy of ROISR was tested with EEG simulations. Two distribution models for both signal and noise sources were studied, one with homogeneous distribution and one with random locations [II]. In the case of random signal source location, the rest of the ROI volume was filled with noise sources. In the case of random signal and noise sources, the noise sources could also be located within the ROI. The correlations in these cases were comparable to those in which ROI was filled with signal sources. Thus the ROISR is also found efficient in estimating the SNR of the

lead in cases where ROI may contain both signal and noise sources. The distribution of noise sources has only a minor effect on the correlations as can be seen, for example, when comparing Cases 1.1 and 2.1 or 3.1 and 4.1 in Table 3. On the basis of these findings the average of sensitivities is a feasible approach when ROISRs are being calculated.

Though the proper selection of ROI size is important, the thesis does not include studies related to the effects of size on correlation. Sinkkilä *et al.* (2008) have shown that the highest correlation in the case of VEP measurement is achieved with a 20 mm radius ROI located at the occipital lobe. The same size for ROI was applied in the studies of this thesis.

The measurable EEG potentials are generated by large groups of neurons and thus the most suitable signal source model applied here would be that with a homogeneous distribution within the ROI (Niedermeyer and Lopes da Silva 1993). The background activity, i.e. noise, has been modelled with both homogeneous and random distributions (de Munck *et al.* 1992; Lutkenhöner 1998a; 1998b). Are these appropriate ways to distribute sources or should there be a combination of the two? One possibility would be to model larger individual volumes describing the activity of brain sections such as the thalamus and cerebellum. In such models the activation of noise sources would be synchronized within the larger volume and not totally random. It has been also noted that there are no purely local or global EEG generators but that there exist connections between local networks and global systems (Niedermeyer and Lopes da Silva 1993; Nunez 2000; Freeman 2004). Thus there would not be just one local ROI. The studies in the present thesis applied only a single ROI volume representing a cortical region where VEPs are produced. Two separate ROIs should be applied in the case of other EPs when responses are generated on both hemispheres, for example, somatosensory responses. The effect of multiple ROIs on the correlation remains a topic for future study.

6.1.2 Effect of EEG source directions

The accuracy of the correlation between ROISR and SNR also depends on the assumption of source directions within the ROI volume as shown in Figure 5.1. On the basis of the theory behind ROISR and EEG simulations presented here, the highest correlation is achieved if the sensitivity distributions are optimally oriented, i.e. parallel to the sources. The simulations show that the accuracy of ROISR in estimating SNR is high (>95%) when the signal source directions are applied correctly to ROISR calculations. The correlations were poorest in cases where the signal sources lie in random directions within the ROI. However, such cases are not realistic because measurable EEG potentials are generated by pyramidal neurons of the same orientation (Niedermeyer and Lopes da Silva 1993). In many cases the measurement set up can be optimally selected and thus the sources within ROI are parallel to the sensitivities. The orientations or magnitudes of the random noise source dipoles cannot be estimated accurately. Thus, in the worst case, the directions of noise sources are parallel to the sensitivities. [I].

The results of the preliminary measurements suggest that the sources producing the P100 component in the primary visual cortex are more likely to be oriented radially than

tangentially because the correlations were higher when sensitivities to the positive y-direction were applied [I]. Similar results for source directions have been achieved in previous studies where cortical dipole sources have been analysed and modelled (Ikeda *et al.* 1998; Di Russo *et al.* 2002; He *et al.* 2002; Di Russo *et al.* 2006).

6.1.3 ROISR in analysing ECG measurements

In the case of the ECG the signal and noise sources are not similar as in EEG. The ECG contains more sequential activity conducting through whole cardiac source medium as the myocardium is a syncytium. In normal heart the segments of the heart are activated in time dependent sequences and there exists no background activity that could be considered as a random noise as in case of EEG. Nevertheless the source region can be divided into segments which present ROI and nonROI volumes.

The applicability of ROISR in estimating the specificity of a measurement was tested against the epicardial dipolar distribution simulations [III]. The simulations were conducted by applying uniform dipole distribution with orientation normal to the epicardial surface over the entire epicardium. The specificity of leads to different segments was analyzed by suppressing the sources of corresponding segment and comparing the resulting potential field with the reference field. The highest ROISR values were located in the same areas as the highest positive potential changes and thus these leads are specific to the changes of activation in ROI. In most cases the highest negative changes in potentials are located in the mid-thoracic region for which the leads are expected to be highly specific to the RV free wall. Suppressing sources in one segment reveals the sources on the opposite side of the myocardium and thus changing the potential on leads which are specific to this opposite region, in these cases RV.

In the ECG case the source directions are better known than in EEG case and thus directions normal to the epicardial surface can, for example, be applied in the ROISR calculation (Selvester *et al.* 1965; Lynn *et al.* 1967). The results showed that there is little effect on the ROISRs or specific leads between cases when the source directions are known or unknown in ROISR calculations. The EEG simulations showed that the highest correlations with unknown source directions are achieved if the sensitivity distribution is optimally oriented. Thus it may be the case here that the specific unipolar leads have optimally oriented sensitivity fields within the corresponding myocardial segment and therefore the effect of source direction in ROISR is minimal.

6.2 Specificity of bipolar EEG leads

The ROISR was applied to study the effect of electrode distance on sensitivity distribution [I]. The effect depends on whether the target source region lies in the cortex or deeper in the brain. Malmivuo and Suihko (2004) showed in their study that in general the short bipolar electrode separations are optimal for measuring sources having tangential orientation while longer electrode distances are specific to radial sources. When sources of interest are deep in the brain the electrode separation should be minimal in order to be specific to the tangential sources and maximal to be specific to the radial sources.

Further in general if the target region is in the cortex the electrode distance should be as short as possible.

Malmivuo *et al.* (1997) report that the short distance three-electrode setup measures the radial component of the cortical sources while, as is shown in this thesis, the short distance bipolar setup measures mostly the tangential component. Thus orientation of the source should be considered in optimization of the measurement setup, and the locations of the measurement electrode and reference electrode(s) should be arranged so that optimal orientation is achieved. According to the findings of the thesis, the optimal bipolar electrode separation for cortical sources of tangential and radial orientation is approximately 30° and less than 20°, respectively. Since the cortical sources have been described with radial dipoles (de Munck *et al.* 1988a) the three electrode setups would probably provide higher specificity and shorter electrode separations. Thus the specificity of the three-electrode setup to cortical sources needs to be analysed with the ROISR method in the future studies.

6.3 Specificities of surface ECG leads on myocardial segments

The ROISR method was applied to investigate the sensitivity distributions of the body surface ECG measurements [III]. The results showed that the leads most specific to different ROI segments were located mainly in the left mid-thoracic region and left back. Using discriminate analysis, Kornreich and colleagues (1986) studied the optimal leads to detect anterior and inferior infarctions. The authors observed that the leads located on the upper thorax show the best capacity for differentiating anterior infarction patients from normal subjects. The same study found that the leads located at the lower left back are the most suitable for distinguishing inferior infarct patients from normal subjects. The same conclusions can be reached from the results of this thesis: the leads on the mid-left thoracic region have high specificity for segments involved in anterior infarction and the leads on the lower left back have high specificity for those involved in inferior infarction.

The results of the thesis show that the posterior leads located around leads 79, 85 and 93 have high ROISR values when ROI is one of the inferior or posterior wall segments (8-12). The inferior and posterior segments are known to be related to inferior and posterior wall disorders. The results of the thesis also confirm the findings of several groups (Matetzky *et al.* 1998; Khaw *et al.* 1999; Somers *et al.* 2003) who have reported that the use of posterior leads (V7-V9) improves the detection of inferior and posterior wall infarction and ischemia.

In addition to the findings of previous clinical studies, the thesis shows that there are no leads which would be highly specific to the septal segments (2 and 3). It is also shown that leads located around V1-V2 are highly specific to the RV wall.

Different optimal leads may be found if only parts of the ECG signal, for example QRS or ST segments, or time-dependent signals are of interest. This is because at each time instant only some parts of the myocardium are active and thus only these would be included in

ROISR analysis. For example, Horácek and colleagues (2001) found optimal unipolar leads for detecting anterior ischemia similar to those presented here, but different leads for inferior- and posterior-related ischemia. Their analysis applied the differences in ST segment.

Since only one model was utilized in this study, the individual optimal leads presented here should be considered as general areas for optimal electrode locations, not as precise locations. Nevertheless, similar lead sets have been found by Lux and colleagues (1978; 1979), Finlay and colleagues (2006) and Barr and colleagues (Barr *et al.* 1971) when selecting an optimal lead set to produce BSPMs. The results of this study and the findings of previous studies suggest that leads in the left mid-thoracic region are specific to certain segments of the LV myocardium and can, therefore, provide independent and discrete information on the activation of these segments. Furthermore, the similarity between ROISR and clinical studies confirms the applicability of the method developed here for analysing ECG measurement setups.

6.4 Implantable ECG measurements

6.4.1 Effects of implantation and implant dimensions on measurement

The average changes in measurement sensitivity of implantable ECG systems were also studied [IV]. The electrode distance was shown to have a major effect on the sensitivity of an active implantable ECG monitor; all other implant dimensions have some effect and these may be of importance when the implant is near the heart or if the implant's dimensions are small. The non-conducting material between electrodes was reported to increase the sensitivity within the heart muscle and thus slightly amplifies the measured signal. Van Dam and van Oosterom (2007) simulated the effects of non-conductive properties and reported that the effects on ECG signal are negligible. There was a difference in electrode positioning between that employed in the thesis and in Van Dam's study where the electrodes were located at the side of the implant and not at the ends.

In the case of more specific lead systems such as for measuring a certain diseased area of the heart, it may be important to observe the local measurement sensitivities in various parts of the heart. In the case of ECG the aim might be to observe the effects of implantation on the P-wave but the average change may not reveal the effects on the sensitivity distribution in the atrium. Here the standard deviation was applied to present possible variation of the local measurement sensitivities. The small change in standard deviation would suggest that the average change in measurement sensitivity describes how all the amplitudes of different ECG waveforms such as P-wave or QRS-complex have changed. In this case all the amplitudes would possibly be decreased or increased depending on the direction of change in sensitivity though the ratio of different peaks would remain the same as in the reference case. In cases where the standard deviation is larger there exists more variation between the changes in local measurement sensitivities. This variation in local sensitivities may affect the morphology of the ECG. However, Zellerhoff *et al.* (2000) and Van Dam and van Oosterom (2007) reported no

significant differences between surface and subcutaneous ECG signals and thus it is likely that the variation in local sensitivities has only a minor effect, at least when electrodes are implanted under fat. The results show that the variation is larger when the electrodes are located under the muscle and this may cause greater changes in the signals.

The results of the thesis also demonstrate that implantation depth has a greater effect on the sensitivity and especially the local sensitivities than the dimensions of the implant. The results presented here show that there is variation in the local sensitivity when electrodes are implanted. It was shown that the deeper the electrodes are implanted under the skin the greater is the effect that can be observed in the changes of local measurement sensitivity. This, however, should be obvious since the implant is closer to the heart and provides a more focused sensitivity distribution.

6.4.2 Effects of implantation location on specificity

The implantation location has been shown to have a variety of effects on the specificity of the measurement. In the thesis the effects of only one orientation and implant size was studied. Some of the tested implantation locations are specific to an individual cardiac segment although most of the locations studied have high specificity to multiple segments.

Similarities in specificities can be found when comparing the results with bipolar implants and unipolar surface leads. For example, unipolar leads and implants in the left mid thoracic region around leads 44 and 65 are both specific to segment 4. Similar results are found for segments 1 and 5 which have specific leads in the left upper anterior thorax. None of the bipolar implantation locations tested was specific to measure septal segments (2 and 3), as was also the case with the unipolar leads.

As discussed earlier, the posterior leads located around locations 79, 85 and 93 are specific to measure the posterior segments (10-11). The implantation locations tested were all on the anterior side but nevertheless there are locations 22 and 44 which can be considered to have increased specificity (ROISR > 2.0) to segment 10.

Although the number of locations tested is limited it could be claimed that the specificities of bipolar implants could also be investigated by studying the unipolar surface leads. Thus the information from clinical studies with unipolar leads could be applied when the objective is to monitor certain specific segments of cardiac muscle with implantable devices.

6.5 Limitations of the studies

The ROISRs in EEG were calculated with a three-layer spherical head model and the ECG studies were conducted with a realistically shaped thorax. Spherical models have been shown to be effective for modelling EEG forward problems and both of the applied geometry models provide a viable platform for studying phenomena (Vanrumste *et al.* 2001; Neilson *et al.* 2005). More accurate results of forward problems and further ROISR

are achieved with individual patient-specific models. Realistic models should, therefore, be applied when the ROISR is applied in practice, for example, in designing patient-specific measurement setups.

Although the spherical model is viable for studying phenomena it has some drawbacks when combined with the measured data. The measurement electrode locations were digitised and fitted on the spherical head model surface. At the centreline and top of the head the brain resembles a sphere but on the sides the brain and the head are not spherical. Thus the fitting of electrodes to the surface of the sphere is not optimal. The radius of the sphere is 92 mm but the human head is not totally spherical, and its radius varies depending on the measurement point. The diameter of the head is longer when measured horizontally from the back to the front than when measured from side to side. There are also differences between individuals. These might decrease the correlation between the modelled ROISRs and measured SNRs although the effects can be considered to be minimal because the tested ROIs were on the centreline of the head.

The models applied here are isotropic. The studies referred to in the literature review have found that anisotropy has only a minor influence on voltage gradients, i.e. sensitivity distributions, within the myocardium. As a result, the effect of anisotropy on the ROISR and further on the results of the thesis is minimal. Nevertheless it would be an interesting topic for future research to investigate how much anisotropy affects ROISR.

6.6 Applications of the methods

The intended use of ROISR is in designing and optimizing new measurement leads and setups by analyzing sensitivity distributions. The ROISR could be applied for estimating which measurement lead is the most specific to measure a certain ROI and thus enabling high SNR. The measurement setups can be evaluated prior to the actual measurements, thereby saving time and cost. The ROISR can be applied, for example, when designing and optimizing the lead systems for EEG studies (Cvetkovic and Cosic 2009).

The ROISR has a high correlation with the SNR of EEG leads when the ROI is correctly selected [I]. The correlations between modelled ROISRs and measured SNRs could be applied in the future to evaluate if the ROI is optimally selected since the correlation is highest when the ROI contains all the signal sources and none of the noise sources. The results of the thesis also show that the correlation between ROISR and SNR is highest when the proper direction of sensitivity is applied in the calculations. The information could be employed to study source directions within the source volumes of interest. These approaches could be potentially applied for source localization purposes.

Averaging of responses (i.e. epochs) is needed in order to obtain high enough SNR, especially in case of EEG EP measurements. Fewer epochs are needed for averaging when the specificity of a measurement is higher. The ROISR method enables designing of more specific measurement configurations. For instance, new reference locations of bipolar EEG measurements could provide more specific measurements and further better SNR. This enables faster measurement protocols while fewer epochs are measured. As an

example, a standard bipolar lead is applied in clinical EEG VEP measurements. The standard lead has reference on forehead and measurement electrode on the back of the head. The electrode separation is around 150°. The results of the thesis show that optimal bipolar measurement with highest specificity has 20° electrode separation if the sources are considered radially-oriented. Thus a short distance bipolar electrode pair located on the back of the head would probably provide measurements with higher SNR.

There exist multiple applications which could benefit from the developed ROISR method such as brain-computer interfaces, EMG-based computer interface. For these applications the method could be applied to design electrode configurations which are highly specific to a certain section of brain or an individual muscle.

Patient-specific lead systems are increasingly in demand as the monitoring of physiological signals becomes more personalized. The ROISR method provides tools for designing personalized aimed-lead configurations. These leads can be either implantable or surface measurements as well as single- or multilead systems.

Studies of the measurement properties of active implants are much harder to conduct than measurements which can be made at the body surface. It is important to have information on the effect of implantation or implant design on measurements in order to facilitate successful and effective implantation. *In vivo* testing and reviewing of implant design by human or animal tests is time-consuming and expensive and the number of iteration rounds is limited.

The methods presented in the thesis are effective and applicable. They allow the sensitivity distribution of the bioelectric measurement lead to be solved in a single calculation by defining only the electrode locations instead of all the sources in the source volume and calculating separately the measured field generated by each source. These properties make it possible to study efficiently the measurement sensitivities of various implantable monitor designs at different implantation locations in the human body. The methods are also applicable in studying how the stimulating currents of other active implantable devices, such as pacemakers or defibrillators, are distributed in the body. There is, thus, far less need for *in vivo* trials during the design process.

The methods presented have potential use in clinical situations when patient-specific measurement setups are being designed. The feasibility and applicability of the methods is restricted by the general modelling issues related to patient-specific model construction and computational resources. The construction of models based on individual image data from MRI or CT scans are expensive and time consuming. Thus the construction of highly detailed models with multiple inhomogeneities and anisotropy is not practicable in a clinical setting. Highly accurate models with millions of elements also require huge computational resources making analysis time consuming, which decreases the applicability and value of the methods in clinical use.

In order to make the methods presented here clinically available, the model geometries should be obtained without the need of expensive imaging modalities and the computational analysis should be conducted in a few minutes. The application of

homogeneous models with the correct shape of volume conductor and placement of source volume has been shown to provide reasonable accuracy in bioelectric forward solutions (Ramanathan and Rudy 2001a; 2001b). A form of patient-specific modelling could be achieved by applying a generic model platform and scaling based on measurements of the volume conductor dimensions. As a result the need for expensive and time-consuming imaging and segmentation could be avoided. The relative position and orientation of the heart could be confirmed by ultrasound, for instance. Combined with multigrid solvers, the forward problems could be analysed with reasonable efficiency and accuracy (Barnes *et al.* 2008).

7 CONCLUSIONS

The purpose of the thesis was to develop a sensitivity distribution analysis method to assess specificity of bioelectric measurement and study implantable ECG measurements by means of sensitivity distributions. The main conclusions of the thesis are as follows:

- The developed ROISR method for analysing the specificity of a measurement was validated with EEG measurements and EEG and ECG simulations.

- The correlation between the ROISR and SNR of EEG measurement was shown to be strong with measurements and simulations. Thus the method developed can be applied to the analysis of relative SNRs of EEG measurements when optimal lead configurations are sought.

- The highest correlations between the ROISR and SNR of EEG measurement is achieved when ROI properly covers the sources of interest and the direction of these sources is correctly estimated in ROISR calculations. These properties have the potential to be applied as tools in source localization.

- It was also demonstrated that the ROISR method provides information on the specificities of ECG leads to detect local pathologies similar to that in previously published clinical studies. The method thus provides an effective means for designing aimed ECG lead configurations for different measurement purposes such as wearable and implantable ECG.

- Similarities between implantable ECG and surface ECG specificities were found. As a result, the previous clinical studies related to the surface measurements could be applied when seeking the implantation locations being aimed at a certain segment of the myocardium.

- The implantation depth has a greater influence on local sensitivities within the myocardium than implant dimensions. This may cause changes to the morphology of the measured ECG.

8 References

Ackerman, M. J. (1991). "The Visible Human Project." J Biocommun **18**(2): 14.

Andrews, T. J., S. D. Halpern and D. Purves (1997). "Correlated Size Variations in Human Visual Cortex, Lateral Geniculate Nucleus, and Optic Tract." J. Neurosci. **17**(8): 2859-2868.

Arthur, R. M., D. B. Geselowitz, S. A. Briller and R. F. Trost (1971). "The path of the electrical center of the human heart determined from surface electrocardiograms." J Electrocardiol **4**(1): 29-33.

Arthur, R. M., D. B. Geselowitz, S. A. Briller and R. F. Trost (1972). "Quadrupole components of the human surface electrocardiogram." Am Heart J **83**(5): 663-77.

Atienza, F. A., J. R. Carrion, A. G. Alberola, J. L. R. Alvarez, J. J. S. Munoz, J. M. Sanchez and M. V. Chavarri (2005). "A probabilistic model of cardiac electrical activity based on a cellular automata system." Revista Espanola De Cardiologia **58**(1): 41-47.

Barnes, D. N., J. S. George and K. T. Ng (2008). "Finite difference iterative solvers for electroencephalography: serial and parallel performance analysis." Med Biol Eng Comput **46**(9): 901-10.

Barr, R. C. (1989). "Genesis of the Electrocardiogram." in Comprehensive Electrocardiology: Theory and Practice in Health and Disease. Eds. P. W. Macfarlane and T. D. V. Lawrie, Pergamon Press. **1:** 129-151.

Barr, R. C., M. S. Spach and G. S. Herman-Giddens (1971). "Selection of the number and positions of measuring locations for electrocardiography." IEEE Trans Biomed Eng **18**(2): 125-38.

Benditt, D. G., C. Ermis, S. Pham, L. Hiltner, A. Vrudney, K. G. Lurie and S. Sakaguchi (2003). "Implantable diagnostic monitoring devices for evaluation of syncope, and tachy- and brady-arrhythmias." J Interv Card Electrophysiol **9**(2): 137-44.

Boersma, L., L. Mont, A. Sionis, E. Garcia and J. Brugada (2004). "Value of the implantable loop recorder for the management of patients with unexplained syncope." Europace **6**(1): 70-6.

Bradley, C. P., A. J. Pullan and P. J. Hunter (2000). "Effects of material properties and geometry on electrocardiographic forward simulations." Ann Biomed Eng **28**(7): 721-41.

Brody, D. A. (1956). "A theoretical analysis of intracavitary blood mass influence on the heart-lead relationship." Circ Res **4**(6): 731-8.

Brooks, D. H. and R. S. MacLeod (1997). "Electrical imaging of the heart." Signal Processing Magazine, IEEE **14**(1): 24-42.

Bruder, H., B. Scholz and K. Abraham-Fuchs (1994). "The influence of inhomogeneous volume conductor models on the ECG and the MCG." Phys Med Biol **39**(11): 1949-68.

Bruno, P., J. Hyttinen, P. Inchingolo, A. Magrofuoco, S. Mininel and F. Vatta (2006). "A FDM anisotropic formulation for EEG simulation." in proc. IEEE Eng Med Biol Soc **1**: 1121-5.

Buist, M. L. and A. J. Pullan (2003). "The effect of torso impedance on epicardial and body surface potentials: a modeling study." IEEE Trans Biomed Eng **50**(7): 816-24.

Burger, H. C. and D. van (1961). "Specific electric resistance of body tissues." Phys Med Biol **5**: 431-47.

Burger, H. C. and J. B. Van Milaan (1946). "Heart-Vector and Leads." Br Heart J **8**(3): 157-61.

Burger, H. C. and J. B. Van Milaan (1947). " Heart-Vector and Leads. Part II." Br Heart J **9**(3): 154-60.

Burger, H. C. and J. B. Van Milaan (1948). "Heart-vector and leads; geometrical representation." Br Heart J **10**(4): 229-33.

Burke, M. C., Z. Song, J. Jenkins, M. Alberts, J. Del Priore and R. Arzbaecher (2003). "Analysis of electrocardiograms for subcutaneous monitors." J Electrocardiol **36 Suppl**: 227-32.

Casson, A. J., S. Smith, J. S. Duncan and E. Rodriguez-Villegas (2008). "Wearable EEG: what is it, why is it needed and what does it entail?" in proc. IEEE Eng Med Biol Soc: 5867-5870

Celesia, G. G., I. Bodis-Wollner, G. E. Chatrian, G. F. Harding, S. Sokol and H. Spekreijse (1993). "Recommended standards for electroretinograms and visual evoked potentials. Report of an IFCN committee." Electroencephalogr Clin Neurophysiol **87**(6): 421-36.

Chrysostomakis, S. I., N. C. Klapsinos, E. N. Simantirakis, M. E. Marketou, D. C. Kambouraki and P. E. Vardas (2003). "Sensing issues related to the clinical use of implantable loop recorders." Europace **5**(2): 143-8.

Cuffin, B. (1991). "Eccentric spheres models of the head." IEEE Trans Biomed Eng **38**(9): 871 - 8.

Cuffin, B. N. (1996). "EEG localization accuracy improvements using realistically shaped head models." IEEE Trans Biomed Eng **43**(3): 299-303.

Cvetkovic, D. and I. Cosic (2009). "EEG inter/intra-hemispheric coherence and asymmetric responses to visual stimulations." Med Biol Eng Comput.

de Jongh, A. L., E. Entcheva, J. A. Replogle and F. J. Claydon (1997). "Effects of cardiac anisotropy on modeling transvenous defibrillation in the human thorax." in proc. IEEE Eng Med Biol Soc: 133-135

de Munck, J. C., B. W. van Dijk and H. Spekreijse (1988a). "Mathematical dipoles are adequate to describe realistic generators of human brain activity." IEEE Trans Biomed Eng **35**(11): 960-6.

de Munck, J. C., B. W. van Dijk and H. Spekreijse (1988b). "Mathematical dipoles are adequate to describe realistic generators of human brain activity." Biomedical Engineering, IEEE Transactions on **35**(11): 960-966.

de Munck, J. C., P. C. Vijn and F. H. Lopes da Silva (1992). "A random dipole model for spontaneous brain activity." IEEE Trans Biomed Eng **39**(8): 791-804.

De Rossi, D. and A. Lymberis (2005). "New generation of smart wearable health systems and applications." IEEE Trans Inf Technol Biomed **9**(3): 293-4.

Di Russo, F., A. Martinez, M. I. Sereno, S. Pitzalis and S. A. Hillyard (2002). "Cortical sources of the early components of the visual evoked potential." Hum Brain Mapp **15**(2): 95-111.

Di Russo, F., S. Pitzalis, T. Aprile, G. Spitoni, F. Patria, A. Stella, D. Spinelli and S. A. Hillyard (2006). "Spatiotemporal analysis of the cortical sources of the steady-state visual evoked potential." Hum Brain Mapp.

Dössel, O., F. Schneider and M. Muller (1998). "Optimization of electrode positions for multichannel electrocardiography with respect to electrical imaging of the heart." in proc. IEEE Eng Med Biol Soc: 71-74

Dower, G. E., A. Yakush, S. B. Nazzal, R. V. Jutzy and C. E. Ruiz (1988). "Deriving the 12-lead electrocardiogram from four (EASI) electrodes." J Electrocardiol **21 Suppl**: S182-7.

Eason, J., J. Schmidt, A. Dabasinskas, G. Siekas, F. Aguel and N. Trayanova (1998). "Influence of anisotropy on local and global measures of potential gradient in computer models of defibrillation." Ann Biomed Eng **26**(5): 840-9.

Einthoven, W., G. Farhr and d. W. A. (1913). "Über die Richtung und die manifeste Grösse der Potentialschwankungen im menschlichen Herzen und über den Einfluss der

Herzlage auf die Form des Elektrokardiogramms." Pflügers Archiv European Journal of Physiology **150**: 275-315.

Epstein, B. R. and K. R. Foster (1983). "Anisotropy in the dielectric properties of skeletal muscle." Med Biol Eng Comput **21**(1): 51-5.

Farwell, D. J., N. Freemantle and A. N. Sulke (2004). "Use of implantable loop recorders in the diagnosis and management of syncope." Eur Heart J **25**(14): 1257-63.

Ferdjallah, M., F. X. Bostick, Jr. and R. E. Barr (1996). "Potential and current density distributions of cranial electrotherapy stimulation (CES) in a four-concentric-spheres model." IEEE Trans Biomed Eng **43**(9): 939-43.

Ferree, T. C., M. T. Clay and D. M. Tucker (2001). "The spatial resolution of scalp EEG." Neurocomputing **38-40**: 1209-1216.

Finlay, D., C. Nugent, M. Donnelly, P. McCullagh and N. Black (2008). "Optimal electrocardiographic lead systems: practical scenarios in smart clothing and wearable health systems." IEEE Trans Inf Technol Biomed **12**(4): 433 - 41.

Finlay, D. D., C. D. Nugent, M. P. Donnelly, R. L. Lux, P. J. McCullagh and N. D. Black (2006). "Selection of optimal recording sites for limited lead body surface potential mapping: a sequential selection based approach." BMC Med Inform Decis Mak **6**: 9.

Finlay, D. D., C. D. Nugent, P. J. McCullagh and N. D. Black (2005). "Mining for diagnostic information in body surface potential maps: a comparison of feature selection techniques." Biomed Eng Online **4**: 51.

Fischell, D., T. Fischell, J. Harwood, R. Fischell and S. Johnson (2008). System for the Detection of Cardiac Events, US20080064973.

Fischmann, E. J. and M. R. Barber (1963). ""Aimed" electrocardiography. Model studies, using a heart consisting of 6 electrically isolated areas." Am Heart J **65**: 628-37.

Fischmann, E. J., M. R. Barber and H. Hedayati (1966). "Aimed electrocardiography with simple bipolar leads. Experimental study of a new concept: surface search for unweighted leads which record the ECG from limited cardiac areas." Circ Res **19**(3): 584-92.

Foster, K. and H. Schwan (1989). "Dielectric properties of tissues and biological materials: a critical review." Crit Rev Biomed Eng **17**(1): 25 - 104.

Frank, E. (1956). "An Accurate, Clinically Practical System For Spatial Vectorcardiography." Circulation **13**(5): 737-749.

Freeman, W. J. (2004). "Origin, structure, and role of background EEG activity. Part 1. Analytic amplitude." Clin Neurophysiol **115**(9): 2077-88.

Fuchs, M., M. Wagner and J. Kastner (2007). "Development of volume conductor and source models to localize epileptic foci." J Clin Neurophysiol **24**(2): 101-19.

Gabriel, C., S. Gabriel and E. Corthout (1996a). "The dielectric properties of biological tissues: I. Literature survey." Phys Med Biol **41**(11): 2231-49.

Gabriel, S., R. W. Lau and C. Gabriel (1996b). "The dielectric properties of biological tissues: II. Measurements in the frequency range 10 Hz to 20 GHz." Phys Med Biol **41**(11): 2251-69.

Gabriel, S., R. W. Lau and C. Gabriel (1996c). "The dielectric properties of biological tissues: III. Parametric models for the dielectric spectrum of tissues." Phys Med Biol **41**(11): 2271-93.

Geddes, L. A. and L. E. Baker (1967). "The specific resistance of biological material--a compendium of data for the biomedical engineer and physiologist." Med Biol Eng **5**(3): 271-93.

Geneser, S., R. Kirby and R. MacLeod (2008). "Application of stochastic finite element methods to study the sensitivity of ECG forward modeling to organ conductivity." IEEE Trans Biomed Eng **55**(1): 31 - 40.

Geselowitz, D. B. (1989)." Theory and simulations of the electrocardiogram." in Comprehensive Electrocardiology: Theory and Practice in Health and Disease. Eds. P. W. Macfarlane and T. D. V. Lawrie, Pergamon Press. **1:** 181-195.

Geselowitz, D. B. and R. M. Arthur (1971). "Derivation of aimed electrocardiographic leads from the multiple expansion." J Electrocardiol **4**(4): 291-8.

Ghanem, R. (2007). "Noninvasive electrocardiographic imaging of arrhythmogenesis: insights from modeling and human studies." J Electrocardiol **40**(6 Suppl): S169 - 73.

Ghosh, S., J. Avari, E. Rhee, P. Woodard and Y. Rudy (2008a). "Noninvasive electrocardiographic imaging (ECGI) of a univentricular heart with Wolff-Parkinson-White syndrome." Heart Rhythm **5**(4): 605 - 8.

Ghosh, S., J. Avari, E. Rhee, P. Woodard and Y. Rudy (2008b). "Noninvasive electrocardiographic imaging (ECGI) of epicardial activation before and after catheter ablation of the accessory pathway in a patient with Ebstein anomaly." Heart Rhythm **5**(6): 857 - 60.

Gordon, R., T. Arola, K. Wendel, O. Ryynänen and J. Hyttinen (2006). "Accuracy of numerical methods by calculating static and quasistatic electric fields." Proceedings of the Estonian Academy of Sciences Engineering **12**(3-2): 262-283.

Gulrajani, R. and G. Mailloux (1983). "A simulation study of the effects of torso inhomogeneities on electrocardiographic potentials, using realistic heart and torso models." Circ Res **52**(1): 45-56.

Gulrajani, R. M., F. A. Roberge and P. Savard (1984). "Moving Dipole Inverse ECG and EEG Solutions." Biomedical Engineering, IEEE Transactions on **BME-31**(12): 903-910.

Gyselinckx, B., J. Penders and R. Vullers (2007). "Potential and challenges of body area networks for cardiac monitoring." J Electrocardiol **40**(6 Suppl): S165-8.

Hallez, H., B. Vanrumste, P. Van Hese, Y. D'Asseler, I. Lemahieu and R. Van de Walle (2005). "A finite difference method with reciprocity used to incorporate anisotropy in electroencephalogram dipole source localization." Phys Med Biol **50**(16): 3787-806.

Haueisen, J., C. Ramon, M. Eiselt, H. Brauer and H. Nowak (1997). "Influence of tissue resistivities on neuromagnetic fields and electric potentials studied with a finite element model of the head." IEEE Trans Biomed Eng **44**(8): 727-35.

Haueisen, J., D. S. Tuch, C. Ramon, P. H. Schimpf, V. J. Wedeen, J. S. George and J. W. Belliveau (2002). "The influence of brain tissue anisotropy on human EEG and MEG." Neuroimage **15**(1): 159-66.

He, B., D. Yao and J. Lian (2002). "High-resolution EEG: on the cortical equivalent dipole layer imaging." Clin Neurophysiol **113**(2): 227-35.

Helmholtz, H. (1853). "Ueber einige Gesetze der Vertheilung elektrischer Ströme in körperlichen Leitern mit Anwendung auf die thierisch-elektrischen Versuche." Annalen der Physik und Chemie **165**(6): 211-233.

Hoekema, R., G. J. Uijen and A. van Oosterom (1999). "On selecting a body surface mapping procedure." J Electrocardiol **32**(2): 93-101.

Hoekema, R., G. H. Wieneke, F. S. Leijten, C. W. van Veelen, P. C. van Rijen, G. J. Huiskamp, J. Ansems and A. C. van Huffelen (2003). "Measurement of the conductivity of skull, temporarily removed during epilepsy surgery." Brain Topogr **16**(1): 29-38.

Horacek, B. M., J. W. Warren, C. J. Penney, R. S. MacLeod, L. M. Title, M. J. Gardner and C. L. Feldman (2001). "Optimal electrocardiographic leads for detecting acute myocardial ischemia." J Electrocardiol **34 Suppl**: 97-111.

Huiskamp, G., M. Vroeijenstijn, R. van Dijk, G. Wieneke and A. C. van Huffelen (1999). "The need for correct realistic geometry in the inverse EEG problem." IEEE Trans Biomed Eng **46**(11): 1281-7.

Hyttinen, J. (1994). "Development of Regional Aimed ECG Leads Especially for Myocardial Ischemia Diagnosis.", Doctoral thesis, Ragnar Granit Institute. Tampere, Tampere University of Technology, 162.

Hyttinen, J., P. Kauppinen, T. Kööbi and J. Malmivuo (1997). "Importance of the Tissue Conductivity Values in Modelling the Thorax as a Volume Conductor." in proc. IEEE Eng Med Biol Soc: 2082-2085

Hyttinen, J. A., J. J. Viik, H. Eskola and J. A. Malmivuo (1995)." Optimization and comparison of derived Frank VECG lead systems employing an accurate thorax model." in proc. Computers in Cardiology: 385-388

Hyttinen, J. A. K., J. A. Malmivuo and S. J. Walker (1993). "Lead field of ECG leads calculated by a computer thorax model-an application of reciprocity." in proc. Computers in Cardiology: 241-244

Ikeda, H., H. Nishijo, K. Miyamoto, R. Tamura, S. Endo and T. Ono (1998). "Generators of visual evoked potentials investigated by dipole tracing in the human occipital cortex." Neuroscience **84**(3): 723-39.

Ives, J. R. (2005). "New chronic EEG electrode for critical/intensive care unit monitoring." J Clin Neurophysiol **22**(2): 119-23.

Jing, L., S. Zhu and B. He (2005). "A finite difference method for solving the three-dimensional EEG forward problem." in proc. IEEE Eng Med Biol Soc **2**: 1540-3.

Johnson, C., R. MacLeod and P. Ershler (1992). "A computer model for the study of electrical current flow in the human thorax." Comput Biol Med **22**(5): 305 - 23.

Johnson, C., R. MacLeod and P. Ershler (1992). "A computer model for the study of electrical current flow in the human thorax." Comput Biol Med **22**(5): 305 - 23.

Johnson, C. R. (1997). "Computational and numerical methods for bioelectric field problems." Crit Rev Biomed Eng **25**(1): 1-81.

Jorgenson, D. B., D. R. Haynor, G. H. Bardy and Y. Kim (1995). "Computational studies of transthoracic and transvenous defibrillation in a detailed 3-D human thorax model." IEEE Trans Biomed Eng **42**(2): 172-84.

Karlon, W., J. Lehr and S. Eisenberg (1994). "Finite element models of thoracic conductive anatomy: sensitivity to changes in inhomogeneity and anisotropy." IEEE Trans Biomed Eng **41**(11): 1010 - 7.

Kauppinen, P., J. Hyttinen, T. Heinonen and J. Malmivuo (1998). "Detailed model of the thorax as a volume conductor based on the visible human man data." J Med Eng Technol **22**(3): 126-33.

Kauppinen, P., J. Hyttinen, P. Laarne and J. Malmivuo (1999a). "A software implementation for detailed volume conductor modelling in electrophysiology using finite difference method." Comput Methods Programs Biomed **58**(2): 191-203.

Kauppinen, P., T. Koobi, S. Kaukinen, J. Hyttinen and J. Malmivuo (1999b). "Application of computer modelling and lead field theory in developing multiple aimed impedance cardiography measurements." J Med Eng Technol **23**(5): 169-77.

Kauppinen, P., T. Salpavaara, A. Salmi, K. Wendel, J. Malmivuo, T. Salmi, T. Silfvast and J. Virtanen (2006). "Emergency EEG - development of quick application on site EEG." in proc. Nordic Congress of Clinical Neurophysiology, Helsinki,

Khaw, K., A. E. Moreyra, A. K. Tannenbaum, M. N. Hosler, T. J. Brewer and J. B. Agarwal (1999). "Improved detection of posterior myocardial wall ischemia with the 15-lead electrocardiogram." Am Heart J **138**(5 Pt 1): 934-40.

Klepfer, R. N., C. R. Johnson and R. S. Macleod (1997). "The effects of inhomogeneities and anisotropies on electrocardiographic fields: a 3-D finite-element study." IEEE Trans Biomed Eng **44**(8): 706-19.

Kornreich, F. (1997). "Clinical Utility of Body Surface Potential Mapping." Cardiac Electrophysiology Review **3**: 304-307.

Kornreich, F. (1998). "Identification of best electrocardiographic leads for diagnosing acute myocardial ischemia." J Electrocardiol **31 Suppl**: 157-63.

Kornreich, F., T. J. Montague, P. M. Rautaharju, P. Block, J. W. Warren and M. B. Horacek (1986). "Identification of best electrocardiographic leads for diagnosing anterior and inferior myocardial infarction by statistical analysis of body surface potential maps." Am J Cardiol **58**(10): 863-71.

Kornreich, F., P. M. Rautaharju, J. Warren, T. J. Montague and B. M. Horacek (1985). "Identification of best electrocardiographic leads for diagnosing myocardial infarction by statistical analysis of body surface potential maps." Am J Cardiol **56**(13): 852-6.

Krasteva, V. T. and S. P. Papazov (2002). "Estimation of current density distribution under electrodes for external defibrillation." Biomed Eng Online **1**(1): 7.

Kybartaite, A., M. Hannula, N. Narra, T. Arola and J. Hyttinen (2006)." Construction of a highly realistic head/brain volume conductor model." in proc. International Conference Biomedical Engineering, Kaunas, Lithuania: 294-299

Laarne, P. (2000)." Implementation of a Realistic Conductivity Model for the Head." Doctoral thesis, Ragnar Granit Institute, Tampere University of Technology, 109.

Laarne, P., P. Kauppinen, J. Hyttinen, J. Malmivuo and H. Eskola (1999). "Effects of tissue resistivities on electroencephalogram sensitivity distribution." Med Biol Eng Comput **37**(5): 555-9.

Laarne, P. H., M. L. Tenhunen-Eskelinen, J. K. Hyttinen and H. J. Eskola (2000). "Effect of EEG electrode density on dipole localization accuracy using two realistically shaped skull resistivity models." Brain Topogr **12**(4): 249-54.

Lai, Y., W. van Drongelen, L. Ding, K. E. Hecox, V. L. Towle, D. M. Frim and B. He (2005). "Estimation of in vivo human brain-to-skull conductivity ratio from simultaneous extra- and intra-cranial electrical potential recordings." Clin Neurophysiol **116**(2): 456-65.

Lantz, G., R. Grave de Peralta, L. Spinelli, M. Seeck and C. M. Michel (2003). "Epileptic source localization with high density EEG: how many electrodes are needed?" Clin Neurophysiol **114**(1): 63-9.

Lemieux, L., A. McBride and J. W. Hand (1996). "Calculation of electrical potentials on the surface of a realistic head model by finite differences." Phys Med Biol **41**(7): 1079-91.

Lou, B., B. Hong, X. Gao and S. Gao (2008). "Bipolar electrode selection for a motor imagery based brain–computer interface." Journal of Neural Engineering **5**(3): 342-349.

Lutkenhöner, B. (1998a). "Dipole source localization by means of maximum likelihood estimation I. Theory and simulations." Electroencephalogr Clin Neurophysiol **106**(4): 314-21.

Lutkenhöner, B. (1998b). "Dipole source localization by means of maximum likelihood estimation. II. Experimental evaluation." Electroencephalogr Clin Neurophysiol **106**(4): 322-9.

Lux, R. L., M. J. Burgess, R. F. Wyatt, A. K. Evans, G. M. Vincent and J. A. Abildskov (1979). "Clinically practical lead systems for improved electrocardiography: comparison with precordial grids and conventional lead systems." Circulation **59**(2): 356-63.

Lux, R. L., C. R. Smith, R. F. Wyatt and J. A. Abildskov (1978). "Limited lead selection for estimation of body surface potential maps in electrocardiography." IEEE Trans Biomed Eng **25**(3): 270-6.

Lymberis, A. and A. Dittmar (2007). "Advanced wearable health systems and applications." IEEE Eng Med Biol Mag **26**(3): 29-33.

Lynn, M. S., A. C. L. Barnard, J. H. Holt and L. T. Sheffield (1967). "A Proposed Method for the Inverse Problem in Electrocardiology." Biophys. J. **7**(6): 925-945.

Macfarlane, P. (1989). "Lead systems." in Comprehensive Electrocardiology: Theory and Practice in Health and Disease. Eds. P. W. Macfarlane and T. D. V. Lawrie, Pergamon Press. **1:** 315-352.

MacLeod, R. S., R. L. Lux and B. Taccardi (1998). "A possible mechanism for electrocardiographically silent changes in cardiac repolarization." J Electrocardiol **30 Suppl**: 114-21.

Malik, M., K. Smits and F. Lindemans (1997). "Computer Modelling of Transthoracic Electric Field During Defibrillation Shocks: An Efficient Finite Difference Implementation." in proc. Computers in Cardiology, 24, 255-258

Malmivuo, J. and R. Plonsey (1995)." Bioelectromagnetism: Principles and Applications of Bioelectric and Biomagnetic Fields." New York, Oxford University Press.

Malmivuo, J., V. Suihko and H. Eskola (1997). "Sensitivity distributions of EEG and MEG measurements." IEEE Trans Biomed Eng **44**(3): 196-208.

Malmivuo, J. A. and V. E. Suihko (2004). "Effect of skull resistivity on the spatial resolutions of EEG and MEG." IEEE Trans Biomed Eng **51**(7): 1276-80.

Matetzky, S., D. Freimark, P. Chouraqui, B. Rabinowitz, S. Rath, E. Kaplinsky and H. Hod (1998). "Significance of ST segment elevations in posterior chest leads (V7 to V9) in

patients with acute inferior myocardial infarction: application for thrombolytic therapy." J Am Coll Cardiol **31**(3): 506-11.

McClelland, A. J., C. G. Owens, I. B. Menown, M. Lown and A. A. Adgey (2003). "Comparison of the 80-lead body surface map to physician and to 12-lead electrocardiogram in detection of acute myocardial infarction." Am J Cardiol **92**(3): 252-7.

McFee, R. and F. D. Johnston (1953). "Electrocardiographic leads. I. Introduction." Circulation **8**(4): 554-68.

McFee, R. and F. D. Johnston (1954a). "Electrocardiographic leads. II. Analysis." Circulation **9**(2): 255-66.

McFee, R. and F. D. Johnston (1954b). "Electrocardiographic leads. III. Synthesis." Circulation **9**(6): 868-80.

Menown, I. B., R. S. Patterson, G. MacKenzie and A. A. Adgey (1998). "Body-surface map models for early diagnosis of acute myocardial infarction." J Electrocardiol **31 Suppl**: 180-8.

Michel, C. M., G. Lantz, L. Spinelli, R. G. De Peralta, T. Landis and M. Seeck (2004). "128-channel EEG source imaging in epilepsy: clinical yield and localization precision." J Clin Neurophysiol **21**(2): 71-83.

Mohr, M. and B. Vanrumste (2003). "Comparing iterative solvers for linear systems associated with the finite difference discretisation of the forward problem in electro-encephalographic source analysis." Med Biol Eng Comput **41**(1): 75-84.

Montague, T. J., E. R. Smith, D. A. Cameron, P. M. Rautaharju, G. A. Klassen, C. S. Felmington and B. M. Horacek (1981). "Isointegral analysis of body surface maps: surface distribution and temporal variability in normal subjects." Circulation **63**(5): 1166-72.

Nadeau, R., P. Savard, R. Gulrajani, R. Cardinal, F. Molin and P. Page (1995). "Clinical applications of BSM." J Electrocardiol **28**(4): 334-5.

Neilson, L. A., M. Kovalyov and Z. J. Koles (2005). "A computationally efficient method for accurately solving the EEG forward problem in a finely discretized head model." Clinical Neurophysiology **116**(10): 2302-2314.

Niedermeyer, E. and F. Lopes da Silva (1993). "Electroencephalography: Basic Principles, Clinical Applications, and Related Fields." Baltimore, Williams and Wilkins.

Nöjd, N., M. Hannula, N. Narra and J. Hyttinen (2008). "Electrode position optimization for facial EMG measurements for human-computer interface." Methods Inf Med **47**(3): 192-7.

Nunez, P. (1981). "Electric Fields of the Brain: The Neurophysics of EEG." New York, Oxford University Press.

Nunez, P. L. (2000). "Toward a quantitative description of large-scale neocortical dynamic function and EEG." Behav Brain Sci **23**(3): 371-98; discussion 399-437.

Oostendorp, T. F., J. Delbeke and D. F. Stegeman (2000). "The conductivity of the human skull: results of in vivo and in vitro measurements." IEEE Trans Biomed Eng **47**(11): 1487-92.

Oostenveld, R. and P. Praamstra (2001). "The five percent electrode system for high-resolution EEG and ERP measurements." Clin Neurophysiol **112**(4): 713-9.

Oster, H. S., B. Taccardi, R. L. Lux, P. R. Ershler and Y. Rudy (1997). "Noninvasive Electrocardiographic Imaging : Reconstruction of Epicardial Potentials, Electrograms, and Isochrones and Localization of Single and Multiple Electrocardiac Events." Circulation **96**(3): 1012-1024.

Panescu, D., J. G. Webster and R. A. Stratbucker (1994). "Modeling current density distributions during transcutaneous cardiac pacing." IEEE Trans Biomed Eng **41**(6): 549-55.

Patterson, R. and L. Wang (1992). Finite difference model of thoracic fields and current flow due to surface applied defibrillation voltages. in proc. Computers in Cardiology 1992. Proceedings., 711-714

Plonsey, R. (1963). "Reciprocity Applied to Volume Conductors and the Ecg." IEEE Trans Biomed Eng **10**: 9-12.

Plonsey, R. and D. B. Heppner (1967). "Considerations of quasi-stationarity in electrophysiological systems." Bull Math Biophys **29**(4): 657-64.

Pruis, G. W., B. H. Gilding and M. J. Peters (1993). "A comparison of different numerical methods for solving the forward problem in EEG and MEG." Physiol Meas **14 Suppl 4A**: A1-9.

Pullan, A., M. L. Buist and L. K. Cheng (2005)."Mathematically modelling the electrical activity of the heart." Singapore, World Scientific.

Puurtinen, M., J. Hyttinen, P. Kauppinen and J. Malmivuo (2004). "Estimation of ECG signal of closely separated bipolar electrodes using thorax models." in proc. IEEE Eng Med Biol Soc, 801-804

Puurtinen, M., J. Hyttinen and J. Malmivuo (2003). "Effect of Interelectrode Distance on ECG Potentials- Modeling Approach vs. Clinical Data." International Journal of Bioelectromagnetism **5**(1): 147-148.

Puurtinen, M., J. Viik and J. Hyttinen (2009a). "Best electrode locations for a small bipolar ECG device: signal strength analysis of clinical data." Ann Biomed Eng **37**(2): 331-6.

Puurtinen, M., J. Viik, N. Takano, J. Malmivuo and J. Hyttinen (2009b). "Estimating the measuring sensitivity of unipolar and bipolar ECG with lead field method and FDM models." Comput Methods Programs Biomed **94**(2): 161-7.

Quyyumi, A. A., T. Crake, L. J. Mockus, C. A. Wright, A. F. Rickards and K. M. Fox (1986). "Value of the bipolar lead CM5 in electrocardiography." Br Heart J **56**(4): 372-6.

Ramanathan, C., R. N. Ghanem, P. Jia, K. Ryu and Y. Rudy (2004). "Noninvasive electrocardiographic imaging for cardiac electrophysiology and arrhythmia." Nat Med **10**(4): 422-8.

Ramanathan, C. and Y. Rudy (2001a). "Electrocardiographic imaging: I. Effect of torso inhomogeneities on body surface electrocardiographic potentials." J Cardiovasc Electrophysiol **12**(2): 229-40.

Ramanathan, C. and Y. Rudy (2001b). "Electrocardiographic imaging: II. Effect of torso inhomogeneities on noninvasive reconstruction of epicardial potentials, electrograms, and isochrones." J Cardiovasc Electrophysiol **12**(2): 241-52.

Ramon, C., P. Schimpf, Y. Wang, J. Haueisen and A. Ishimaru (2002). "The effect of volume currents due to myocardial anisotropy on body surface potentials." Phys Med Biol **47**(7): 1167-84.

Ramon, C., P. H. Schimpf and J. Haueisen (2006). "Influence of head models on EEG simulations and inverse source localizations." Biomed Eng Online **5**: 10.

Ramon, C., Y. Wang, J. Haueisen, P. Schimpf, S. Jaruvatanadilok and A. Ishimaru (2000). "Effect of myocardial anisotropy on the torso current flow patterns, potentials and magnetic fields." Phys Med Biol **45**(5): 1141-50.

Raz, J., B. Turetsky and G. Fein (1988). "Confidence intervals for the signal-to-noise ratio when a signal embedded in noise is observed over repeated trials." IEEE Trans Biomed Eng **35**(8): 646-9.

Riistama, J., J. Väisänen, S. Heinisuo, H. Harjunpää, S. Arra, K. Kokko, M. Mäntylä, M. Kellomäki, J. Vanhala, P. Heino, J. Hyttinen, J. Lekkala, J. Kaihilahti and O. Vainio (2007). "Wireless And Inductively Powered Implant For Measuring Electrocardiogram." Med Biol Eng Comput **45**(12): 1163-1174.

Riistama, J., J. Väisänen, S. Heinisuo, J. Lekkala and J. Hyttinen (2005). "Introducing a Wireless, Passive and Implantable Device to Measure ECG." in proc. IFMBE proceedings of The 3rd European Medical and Biological Engineering Conference, Prague, IFMBE, 11,

Rudy, Y. and R. Plonsey (1979). "The eccentric spheres model as the basis for a study of the role of geometry and inhomogeneities in electrocardiography." IEEE Trans Biomed Eng **26**(7): 392-9.

Rudy, Y., R. Plonsey and J. Liebman (1979). "The effects of variations in conductivity and geometrical parameters on the electrocardiogram, using an eccentric spheres model." Circ Res **44**(1): 104 - 11.

Rush, S., J. A. Abildskov and McFeer (1963). "Resistivity of body tissues at low frequencies." Circ Res **12**: 40-50.

Rush, S. and D. A. Driscoll (1968). "Current distribution in the brain from surface electrodes." Anesth Analg **47**(6): 717-23.

Rush, S. and D. A. Driscoll (1969). "EEG electrode sensitivity--an application of reciprocity." IEEE Trans Biomed Eng **16**(1): 15-22.

Russell, J. K. and S. Gehman (2007). "Early experience with a novel ambulatory monitor." J Electrocardiol **40**(6 Suppl): S160-4.

Ryynänen, O. R. M., J. A. K. Hyttinen and J. A. Malmivuo (2006). "Effect of measurement noise and electrode density on the spatial resolution of cortical potential distribution with different resistivity values for the skull." Biomedical Engineering, IEEE Transactions on **53**(9): 1851-1858.

Sachse, F. B. (2004). "Computational Cardiology: Modeling of Anatomy Electrophysiology, and Mechanics." Berlin, Springer.

Sachse, F. B., C. D. Werner, K. Meyer-Waarden and O. Dössel (2000). "Development of a human body model for numerical calculation of electrical fields." Comput Med Imaging Graph **24**(3): 165-71.

Sarkar, S., D. Ritscher and R. Mehra (2008). "A detector for a chronic implantable atrial tachyarrhythmia monitor." IEEE Trans Biomed Eng **55**(3): 1219-24.

Schneider, A. L. (2006). "Subdermal needle electrodes: an option for emergency ("stat") EEGs." Am J Electroneurodiagnostic Technol **46**(4): 363-8.

Seitz, S., G. Seemann and O. Dössel (2008). "Influence of Tissue Anisotropy on the Distribution of Defibrillation Fields." in proc. Computers in Cardiology, 35, 489-492

Selvester, R. H., C. R. Collier and R. B. Pearson (1965). "Analog Computer Model of the Vectorcardiogram." Circulation **31**: 45-53.

Selvester, R. H., J. C. Solomon and T. L. Gillespie (1968). "Digital computer model of a total body electrocardiographic surface map. An adult male-torso simulation with lungs." Circulation **38**(4): 684-90.

Sinkkilä, L. (2010)."Region of Interest Sensitivity Ratio in EEG Sensitivity Analysis.", Master of Science Thesis, Department of Biomedical Engineering. Tampere, Tampere University of Technology

Sinkkilä, L., J. Väisänen, O. Väisänen and J. Hyttinen (2008). "Effects of ROI size on correlation between ROISR and SNR." in proc. 14th Nordic Baltic Conference on Biomedical Engineering, Riga, 327-330

Somers, M. P., W. J. Brady, D. C. Bateman, A. Mattu and A. D. Perron (2003). "Additional electrocardiographic leads in the ED chest pain patient: right ventricular and posterior leads." Am J Emerg Med **21**(7): 563-73.

Song, Z., J. Jenkins, M. Burke and R. Arzbaecher (2004). "The feasibility of ST-segment monitoring with a subcutaneous device." J Electrocardiol **37 Suppl**: 174-9.

Startt/Selvester, R. H., G. S. Wagner and R. E. Ideker (1989). Myocardial Infaction. in Comprehensive Electrocardiology: Theory and Practice in Health and Disease. Eds. P. W. Macfarlane and T. D. V. Lawrie, Pergamon Press. **1:** 565-629.

Takano, N. (2002)." Reduction of ECG Leads and Equivalent Sources Using Orthogonalization and Clustering Techniques.", Doctoral thesis, Ragnar Granit Institute. Tampere, Tampere University of Technology, 302.

Tragardh, E., H. Engblom and O. Pahlm (2006). "How many ECG leads do we need?" Cardiology Clinics **24**(3): 317-330.

TransomaMedical The Sleuth Implantable ECG Monitoring System.

Wagner, G. S., M. J. Cowan, N. C. Flowers, L. E. Ginzton, R. E. Ideker, M. M. Laks, R. H. Selvester and S. R. Swiryn (1984). Report of Committee on Nomenclature of Myocardial Wall Segments. in proc. Computerized Interpretation of Electrocardiograms VII proc. Engineering Foundation Conference, New York, 361-369

Walker, S. and D. Kilpatrick (1987). "Forward and inverse electrocardiographic calculations using resistor network models of the human torso." Circ Res **61**(4): 504-513.

van Dam, P. and A. van Oosterom (2005). "Volume conductor effects involved in the genesis of the P wave." Europace **7 Suppl 2**: 30 - 8.

van Dam, P. M. and A. van Oosterom (2007). "Analysing the potential of Reveal for monitoring cardiac potentials." Europace **9 Suppl 6**: vi119-23.

van Oosterom, A. (1989). "Cell Models-Macroscopic Source Descriptions." in Comprehensive Electrocardiology: Theory and Practice in Health and Disease. Eds. P. W. Macfarlane and T. D. V. Lawrie, Pergamon Press. **1:** 155-180.

van Oosterom, A. and G. J. Huiskamp (1989). "The effect of torso inhomogeneities on body surface potentials quantified using "tailored" geometry." J Electrocardiol **22**(1): 53-72.

Wang, Y., D. R. Haynor and Y. Kim (2001). "An investigation of the importance of myocardial anisotropy in finite-element modeling of the heart: methodology and application to the estimation of defibrillation efficacy." IEEE Trans Biomed Eng **48**(12): 1377-89.

Vanrumste, B., G. Van Hoey, R. Van de Walle, M. R. D'Have, I. A. Lemahieu and P. A. Boon (2001). "The validation of the finite difference method and reciprocity for solving the inverse problem in EEG dipole source analysis." Brain Topogr **14**(2): 83-92.

Watson, J. D. G. (2000). "The Human Visual System." in Brain Mapping: The Systems. Eds. A. W. Toga and J. C. Mazziotta. San Diego, Academic press**:** 263-289.

Watson, J. D. G. (2000). "The Human Visual System." in Brain Mapping: The Systems. Eds. A. W. Toga and J. C. Mazziotta. San Diego, Academic press**:** 263-289.

Vehkaoja, A. and J. Lekkala (2004). "Wearable wireless biopotential measurement device." in proc. IEEE Eng Med Biol Soc: 2177-2179

Wei, D., O. Okazaki, K. Harumi, E. Harasawa and H. Hosaka (1995). "Comparative simulation of excitation and body surface electrocardiogram with isotropic and anisotropic computer heart models." IEEE Trans Biomed Eng **42**(4): 343-57.

Wendel, K., N. G. Narra, M. Hannula, P. Kauppinen and J. Malmivuo (2008). "The influence of CSF on EEG sensitivity distributions of multilayered head models." IEEE Trans Biomed Eng **55**(4): 1454-6.

Werner, C. D., F. B. Sachse and O. Dossel (2000). "Electrical Excitation Propagation in the Human Heart." International Journal of Bioelectromagnetism **2**(2).

Wilber, D. (2007 Aug). "Electrocardiographic imaging: new tool for interventional electrophysiology, or just another pretty picture?" Heart Rhythm **4**(8): 1085 - 6.

Wilson, F. N., F. D. Johnston, A. G. Macleod and P. S. Barker (1934). "Electrocardiograms that represent the potential variations of a single electrode,." American Heart Journal **9**(4): 447-458.

Wolters, C. H., A. Anwander, X. Tricoche, D. Weinstein, M. A. Koch and R. S. MacLeod (2006). "Influence of tissue conductivity anisotropy on EEG/MEG field and return current computation in a realistic head model: a simulation and visualization study using high-resolution finite element modeling." Neuroimage **30**(3): 813-26.

Väisänen, O. and J. Malmivuo (2009). "Improving the SNR of EEG generated by deep sources with weighted multielectrode leads." Journal of Physiology-Paris, **103**(6): 306-314.

Yang, F. and R. P. Patterson (2008). "A simulation study on the effect of thoracic conductivity inhomogeneities on sensitivity distributions." Ann Biomed Eng **36**(5): 762-8.

Zellerhoff, C., E. Himmrich, D. Nebeling, O. Przibille, B. Nowak and A. Liebrich (2000). "How can we identify the best implantation site for an ECG event recorder?" Pacing Clin Electrophysiol **23**(10 Pt 1): 1545-9.

Zhou, H. and A. van Oosterom (1992). "Computation of the potential distribution in a four-layer anisotropic concentric spherical volume conductor." IEEE Trans Biomed Eng **39**(2): 154-8.

9 ORIGINAL PUBLICATIONS

[I] J. Väisänen, O. Väisänen, J. Malmivuo, J. Hyttinen: “New Method for Analysing Sensitivity Distributions of Electroencephalography Measurements” Med. Bio. Eng. Comp., vol 46. (2) pp. 101-108, 2008

[II] J. Väisänen, J. Malmivuo, J.Hyttinen: “Correlation between Signal-to-Noise Ratios and Region of Interest Sensitivity Ratios of Bipolar EEG Measurements” Med Bio. Eng Comp., vol 46. (4) pp. 381-389, 2008

[III] J. Väisänen, J.Hyttinen: “Region of Interest Sensitivity Ratio in Analyzing Sensitivity Distributions of Electrocardiographic Measurements” Ann. Biomed. Eng., vol 36. (4), pp.692-701, 2009

[IV] J. Väisänen, J. Hyttinen, J. Malmivuo: “Finite Difference and Lead Field Methods in Designing of Implantable ECG Monitor” Med. Bio. Eng Comp, vol. 44, (10), pp. 857-864, 2006

[V] J. Väisänen, J. Hyttinen, and J. Malmivuo, ”Analysing Specificity of a Bipolar ECG Implant to 12 Segments of the Left Ventricle”, in proc. , Computers in Cardiology 2006, Valencia, (33), pp. 753-756, 2006